Check for updates

*Natural Resource Modeling*

WILEY

Natural Resource Modeling

OPEN ACCESS

# Cooperative and Non-Cooperative Solutions in a Dynamic Model of Forest Management

Seyedalireza Seyedi[1] | Elettra Agliardi[1] | Anastasios Xepapadeas[1,2]

[1]Department of Economics, University of Bologna, Bologna, Italy | [2]Athens University of Economics and Business, Athens, Greece

**Correspondence:** Elettra Agliardi (elettra.agliardi@unibo.it)

**Received:** 2 August 2025 | **Revised:** 27 May 2026 | **Accepted:** 2 June 2026

**Funding:** Ministero dell'Università e della Ricerca, Grant/Award Numbers: 20223PNJ8K_002, Sector SH7

**Keywords:** biodiversity | finite-horizon cooperative governance | forest dynamics

## ABSTRACT

This study develops a deterministic finite-horizon bioeconomic control model linking forest biomass, biodiversity, cumulative harvesting pressure, and disturbance-motivated expected biodiversity losses. Biodiversity is modeled as a productive state variable that feeds back into biomass growth, while cumulative harvesting pressure records the ecological memory of past extraction. Disturbance risk is introduced through a compound Poisson motivation but enters the solved control systems only through a deterministic expected-loss term, so the analysis should be interpreted as an expected-drift benchmark rather than a full stochastic-control treatment. The model compares three governance regimes: a noncooperative open-loop Nash benchmark with free terminal states, a cooperative regulator with fixed terminal ecological targets, and a cooperative regulator with free terminal states. Numerical solutions show that the noncooperative benchmark generates stronger biomass decline and higher cumulative harvesting pressure because private harvesters do not internalize biodiversity's contribution to future productivity. Cooperative regimes generate more favorable ecological trajectories and objective-value outcomes in the calibrated benchmark, with endpoint design shaping terminal adjustments. Local sensitivity analysis, based on regime-consistent perturbations of the boundary-value problems, indicates that the noncooperative benchmark is more responsive to cumulative-pressure damage and expected disturbance losses, while cooperative regimes display smoother or more endpoint-specific responses. Overall, the results highlight the importance of treating biodiversity as productive ecological capital and of accounting for governance structure and endpoint design in dynamic forest-management models.

## 1 | Introduction

Reconciling short-run harvesting incentives with long-run ecological sustainability remains a central challenge in forest management. Forest ecosystems provide marketable products such as timber, but they also generate public ecological services, including carbon sequestration, hydrological regulation, habitat provision, and biodiversity maintenance (Spittlehouse and Stewart 2004; Puettmann et al. 2012). Since Faustmann (1849) foundational rotation model, forest economics has developed tools for analyzing intertemporal harvest decisions under timber-price uncertainty, disturbance risk, and non-market values (Lembersky 1978; Reed 1984; Snyder and Bhattacharyya 1990; Chadès and Bouteiller 2005). Yet many forest bioeconomic models still treat biodiversity as external to the production process, rather than as an ecological state variable that affects forest productivity itself.

This omission is important because ecological evidence shows that species diversity, functional diversity, and structural heterogeneity can enhance forest productivity, carbon storage, and ecosystem stability through mechanisms such as complementarity, facilitation, and insurance effects (Tilman et al. 1996; Cardinale et al. 2012; Brockerhoff et al. 2017). If biodiversity

This is an open access article under the terms of the Creative Commons Attribution License, which permits use, distribution and reproduction in any medium, provided the original work is properly cited.

© 2026 The Author(s). *Natural Resource Modeling* published by Wiley Periodicals LLC.

**Summary**

- Finite-horizon optimal control model linking forest biomass, biodiversity, and harvesting dynamics.
- Cooperative versus noncooperative management internalizing biodiversity values.
- Flexible versus fixed terminal constraints in governance mandates.

contributes to biomass regeneration, then biodiversity loss is not only an ecological concern but also an economic one: it can reduce future productivity and alter the intertemporal value of standing biomass. Standard harvest models that treat biodiversity as exogenous may therefore understate both ecological risk and the long-run value of conservation.

A second limitation concerns governance. Forest extraction often involves strategic interactions among multiple agents, while ecological outcomes depend on cumulative harvesting pressure and delayed feedbacks. Flexible management and demographic modeling have improved the ecological realism of dynamic resource models (Caswell 1989; Walters and Holling 1990; Franklin et al. 2000; Grimm et al. 2005; Allen et al. 2011), but the interaction between biodiversity-dependent productivity, cumulative harvesting pressure, and alternative governance regimes remains less developed. In particular, it is important to understand how decentralized harvesting differs from cooperative management when biodiversity affects productivity and when endpoint design constrains, or permits, intertemporal adjustment.

This paper addresses these issues by developing a deterministic finite-horizon bioeconomic model of biomass harvesting, biodiversity conservation, and cumulative harvesting pressure. Biodiversity is modeled as a dynamic state variable that enters the biomass growth rate and is itself affected by cumulative harvesting pressure. Disturbance risk is introduced only as a motivation for a deterministic expected-loss term in the biodiversity equation; the paper does not solve a full stochastic-control problem or simulate stochastic sample paths. This expected-drift reduction provides a tractable way to incorporate disturbance-motivated biodiversity losses while keeping the solved control systems deterministic.

The model compares three governance regimes: a noncooperative open-loop Nash equilibrium with free terminal states, a cooperative regulator with fixed terminal ecological targets, and a cooperative regulator with free terminal states implemented through transversality conditions. Relative to forest models that incorporate disturbance or non-timber values while treating biodiversity as external to biomass growth, the present framework endogenizes biodiversity as a productive state variable and links it to cumulative harvesting pressure (Reed 1984; Touza et al. 2008). It also connects forest-harvest dynamics to biodiversity-economics models that emphasize ecological capital, stock externalities, and uncertainty (Brock and Xepapadeas 2003; Baumgärtner et al. 2006; Vardas and Xepapadeas 2010; Xepapadeas 2022).

The numerical analysis shows how governance structure and endpoint design affect harvest paths, biomass dynamics, biodiversity recovery, cumulative harvesting pressure, and shadow values. In the calibrated deterministic benchmark, cooperative regimes generate more favorable ecological trajectories than the noncooperative benchmark because they internalize biodiversity's contribution to future productivity. The fixed-endpoint cooperative regime enforces terminal ecological targets but can induce stronger boundary adjustments, whereas the free-endpoint cooperative regime allows smoother intertemporal adaptation. These results are interpreted as comparative mechanisms within the specified deterministic model, not as global robustness claims or as prescriptions for a complete policy instrument.

The shadow-value differences between the noncooperative and cooperative regimes provide a model-based diagnostic of incentive misalignment. They indicate the direction and timing of potential incentive corrections that could align private harvesting incentives with cooperative ecological valuation. This logic is related to Pigouvian reasoning, but the model does not design or evaluate an implementable tax scheme. In practice, enforcement constraints, credit limitations, and incomplete property rights may make direct dynamic pricing difficult, especially in tropical forest contexts. Instruments such as Payments for Ecosystem Services, conservation subsidies, and conservation-linked finance may therefore provide more feasible ways to approximate cooperative incentives by rewarding avoided degradation or ecological performance.

The contribution of the paper is threefold. First, it incorporates biodiversity directly into biomass productivity, treating biodiversity as a dynamic productive input rather than a static constraint or amenity. Second, it introduces cumulative harvesting pressure as an ecological memory state that links current extraction to future biodiversity dynamics. Third, it compares noncooperative and cooperative governance under alternative endpoint designs, thereby showing how strategic incentives and terminal restrictions shape ecological and economic trajectories. These contributions build on the broader literature on biodiversity, ecosystem services, and dynamic resource economics (Brock and Xepapadeas 2002, 2003; Naeem et al. 2009; Vardas and Xepapadeas 2010) and are consistent with policy discussions emphasizing biodiversity valuation and ecosystem-based governance, including frameworks associated with IPBES[1] (IPBES 2019; Bongaarts 2019).

The paper is organized as follows. Section 2 reviews the related literature. Section 3 presents the model, including the ecological dynamics, disturbance-motivated expected-loss term, and governance regimes. Section 4 reports the numerical results and model-based policy implications. Section 5 discusses the findings and concludes. Appendix A provides steady-state and local-property benchmarks for the deterministic ecological subsystem. Appendix B examines nonlinear biodiversity dynamics. Supporting Information S1 reports local sensitivity analysis, Supporting Information S2 documents calibration and numerical implementation, and Appendix C provides the Mathematica code.

## 2 | Literature

The economic foundations of forest-harvest modeling trace back to Faustmann (1849), who formulated timber rotation as



19397445, 2026, 3, Downloaded from https://onlinelibrary.wiley.com/doi/10.1111/nrm.70037 by CochraneItalia, Wiley Online Library on [04/07/2026]. See the Terms and Conditions (https://onlinelibrary.wiley.com/terms-and-conditions) on Wiley Online Library for rules of use; OA articles are governed by the applicable Creative Commons License

an intertemporal investment problem based on discounted future revenues. Later work refined this framework by incorporating replanting costs, variable interest rates, and fiscal instruments, showing how establishment costs, discounting, and policy parameters affect optimal rotation length (Hyytiäinen and Tahvonen 2003). Although these contributions established the canonical economic logic of forest management, they generally treated forest growth as deterministic and ecological complexity as either exogenous or highly simplified.

A second strand of the literature introduced uncertainty into forest optimization. Clarke and Reed (1989) jointly modeled price and stock dynamics using geometric Brownian motion and derived stochastic stopping rules that balance timber-price volatility against biological growth. Willassen (1998) extended this line of work using impulse-control methods, while Buongiorno (2001) applied Markov decision processes to forest-policy simulation under uncertainty. Earlier, Lembersky (1978) showed how Markov decision processes could be used to manage forest dynamics under probabilistic state transitions, and Chadès and Bouteiller (2005) developed related multi-agent forest-management applications in a decision-theoretic framework. These approaches substantially enriched forest decision models, but biodiversity was generally not modeled as a state variable that directly affects biomass productivity.

Another important branch of the literature incorporated abrupt ecological disturbances. Routledge (1980) and Reed (1984) showed that wildfire risk can shorten optimal rotation ages, while Thorsen and Helles (1998) linked windthrow risk to stand structure. Loisel (2014) further incorporated storm and pest damages into stochastic forest-management frameworks. These studies introduced ecological risk into forest economics, but biodiversity typically entered, if at all, as an affected ecological attribute rather than as an endogenous component of the productivity process.

As forest economics broadened toward ecosystem services, non-timber values became increasingly important. Snyder and Bhattacharyya (1990) modeled recreation benefits that vary with stand age; Swallow and Wear (1993) incorporated wildlife habitat preferences; and Koskela and Ollikainen (2001) analyzed private and public harvesting under spatial and temporal interdependence. Related forest-management models examined thinning, rotation, and stand-management decisions under more general management objectives (Haight and Monserud 1990; Cao et al. 2006; Clark 2010). In most of these settings, however, amenities and ecological values affected the objective function rather than feeding back directly into biological growth.

More flexible harvesting models emerged through uneven-aged management, selective logging, and continuous-effort formulations. Schreuder (1971) analyzed the joint determination of thinning schedules and rotation length in an even-aged forest. Montgomery and Adams (1995) used Hamilton–Jacobi–Bellman methods to characterize steady-state logging rules under continuous effort, while Touza et al. (2008) applied variational inequalities to dynamic harvesting decisions. These models allowed for richer management structures and regeneration processes, but biodiversity feedbacks were still generally not specified as an explicit driver of biomass growth.

Strategic interaction adds a further layer of complexity when forests are managed under fragmented property rights, decentralized extraction, or open-access pressures. Differential-game methods provide a natural framework for analyzing intertemporal externalities among strategic agents (Başar and Olsder 1999). Yet relatively few forest bioeconomic models combine strategic harvesting with biodiversity-dependent productivity and cumulative ecological pressure. This omission is important because ecological research shows that biodiversity can enhance productivity, nutrient cycling, structural stability, and resilience. Tilman et al. (1996), Cardinale et al. (2012), and Brockerhoff et al. (2017) provide evidence that species richness and structural heterogeneity can improve ecosystem functioning. Excluding such mechanisms may therefore understate both ecological resilience and the long-run economic value of conservation.

Disturbance ecology also motivates the inclusion of abrupt ecological losses. Wildfires, pest outbreaks, windthrow, pathogen incursions, and extreme weather events can alter biodiversity and ecosystem functioning over short time scales (Turner 2010; Johnstone et al. 2016). Stochastic-control and jump-process methods provide tools for representing such events in dynamic models, including jump-diffusion approaches and catastrophe-risk formulations in renewable-resource economics (Reed 1988; Øksendal and Sulem 2007; Allen 2010). In the present paper, this literature motivates the disturbance component of the biodiversity equation. However, the analysis does not solve a full stochastic-control problem. Instead, the disturbance process is reduced to a deterministic expected-drift term that enters the finite-horizon control system as an expected biodiversity-loss component.

Table 1 situates the present contribution relative to selected benchmark studies in forest economics, biodiversity economics, and dynamic resource modeling. The table compares whether these studies incorporate four structural ingredients emphasized here: biodiversity-dependent biomass productivity $r(B(t))$, a cumulative harvesting-pressure state $Z(t)$, an explicit Nash–planner comparison, and finite-horizon endpoint design. The comparison is not intended as an exhaustive literature review; rather, it identifies the modeling ingredients that distinguish the present framework from closely related approaches.

Recent work by Agliardi et al. (2024) moves toward a more integrated ecological-economic perspective by examining biodiversity preservation under ambiguity, irreversibility, and regulatory constraints. The present study is complementary but distinct. It develops a deterministic finite-horizon bioeconomic model in which biodiversity enters the biomass growth function, while biodiversity itself is affected by cumulative harvesting pressure and an expected disturbance-loss term. The model compares three governance regimes: noncooperative harvesting with free terminal states, cooperative regulation with fixed terminal constraints, and cooperative regulation with free terminal states implemented through transversality conditions.

Methodologically, the paper applies Pontryagin's Maximum Principle to derive the open-loop Nash and cooperative benchmark systems (Corriga et al. 1988; Xepapadeas 2022). Substantively, it shows how biodiversity-dependent



19397445, 2026, 3, Downloaded from https://onlinelibrary.wiley.com/doi/10.1111/nrm.70037 by CochraneItalia, Wiley Online Library on [04/07/2026]. See the Terms and Conditions (https://onlinelibrary.wiley.com/terms-and-conditions) on Wiley Online Library for rules of use; OA articles are governed by the applicable Creative Commons License

**TABLE 1** | Comparison of core modeling ingredients across selected benchmark studies.

| Selected benchmark | Biodiversity-dependent biomass productivity $r(B(t))$ | Cumulative harvesting-pressure state $Z(t)$ | Strategic structure: Nash versus planner | Finite-horizon endpoint design |
|---|---|---|---|---|
| Reed (1984) | — | — | — single decision-maker rotation problem | — |
| Touza et al. (2008) | —[a] | — | — | — |
| Brock and Xepapadeas (2002, 2003) | ◐ biodiversity valuation/ecosystem management; not a forest biomass-productivity channel | — | — | — |
| Clark (2010) | ◐ general renewable-resource growth framework; biodiversity–growth feedback is not a standard forest component | — | ◐ strategic settings are covered in resource economics generally, but not the explicit Nash–planner comparison used here | — |
| Chadès and Bouteiller (2005) | — | — | ◐ multi-agent decision setting; not an explicit open-loop Nash versus planner comparison as used here | — |
| Agliardi et al. (2024) | ◐ biodiversity preservation under uncertainty/ambiguity; not a forest biomass-growth feedback | — | — | — |
| This study | ✓ | ✓ | ✓ open-loop Nash benchmark versus cooperative planner | ✓ fixed-endpoint versus free-endpoint finite-horizon implementation |

*Note:* The table indicates whether selected benchmark studies incorporate, in the sense used here, biodiversity-dependent biomass productivity, cumulative harvesting pressure, an explicit Nash–planner comparison, and finite-horizon endpoint design. ✓: explicitly present as a core structural ingredient; —: not modeled in the indicated sense; ◐: present in a related form, but not as the specific structural ingredient defined in the column heading.

[a]Touza et al. (2008) incorporate ecological interactions and non-timber forest benefits, but they do not model biodiversity as an explicit state variable $B(t)$ entering biomass growth through a biodiversity-dependent growth rate $r(B(t))$, as in the present specification.



19397445, 2026, 3, Downloaded from https://onlinelibrary.wiley.com/doi/10.1111/nrm.70037 by CochraneItalia, Wiley Online Library on [04/07/2026]. See the Terms and Conditions (https://onlinelibrary.wiley.com/terms-and-conditions) on Wiley Online Library for rules of use; OA articles are governed by the applicable Creative Commons License

productivity, cumulative harvesting pressure, and endpoint design jointly shape biomass, biodiversity, harvesting paths, and shadow values. The resulting divergence between decentralized and cooperative shadow values provides a model-based diagnostic for incentive misalignment, while the deterministic expected-loss term incorporates disturbance-motivated biodiversity losses without presenting the analysis as a full stochastic-control treatment.

## 3 | The Model

This study develops a finite-horizon bioeconomic model of biomass harvesting, biodiversity conservation, and forest ecosystem sustainability in a spatially homogeneous forest. The economy consists of $n$ rational harvesting agents, indexed by $i = 1,2, \ldots, n$. Each agent chooses a nonnegative harvesting path $u_i(t)$ over the planning horizon $t \in [0, T]$. In the numerical experiments, $T = 20$, a horizon long enough to display transitional and terminal effects while maintaining numerical stability in the associated boundary-value computations. The same horizon is used across governance regimes to ensure comparability.

Spatial homogeneity implies that biomass and biodiversity are uniformly distributed across the forest. The system can therefore be represented by aggregate state variables. Let $x(t) \geq 0$ denote standing biomass, $B(t) \geq 0$ denote the biodiversity or ecological-functionality index, and $Z(t) \geq 0$ denote cumulative harvesting pressure, interpreted as the ecological memory of past extraction.

The natural growth of standing biomass is first written in generalized nonlinear form as

$$F(x) = \alpha x(t) - \beta x(t)^{\theta+1} \tag{1}$$

Consistent with standard population-ecology modeling, we set $\theta = 1$, $\alpha = r(B(t))$, and $\beta = r(B(t))/K$, where $K > 0$ is the biomass carrying capacity and $r(B(t))$ is the biodiversity-dependent intrinsic growth rate of biomass. Incorporating aggregate harvesting gives

$$\dot{x}(t) = r(B(t))x(t)\left(1 - \frac{x(t)}{K}\right) - \sum_{i=1}^{n} u_i(t) \tag{2}$$

The function $r(B(t))$ links ecological condition to forest regenerative capacity. This specification is motivated by evidence that biodiversity enhances ecosystem functioning, often in a nonlinear way. Tilman et al. (1996) describe saturating productivity effects of species richness; Loreau and Hector (2001) identify complementarity and selection effects as mechanisms linking biodiversity to ecosystem functioning; and Cardinale et al. (2012) synthesize evidence supporting nonlinear, concave biodiversity–ecosystem-service relationships. We therefore specify

$$r(B(t)) = A(B(t))^{\zeta}, A > 0, 0 < \zeta \leq 1. \tag{3}$$

where $A$ is a productivity scale parameter and $\zeta$ is the elasticity of biomass growth with respect to biodiversity. When $\zeta < 1$, biodiversity raises biomass productivity at a diminishing marginal rate; when $\zeta = 1$, the relationship is linear.

Biodiversity is also dynamic. Following the bioeconomic perspective emphasized by Baumgärtner et al. (2006), biodiversity evolves according to

$$\dot{B}(t) = G(B(t), Z(t)), \tag{4}$$

where $G$ is the biodiversity-growth function and $Z(t)$ measures cumulative harvesting pressure. In its general form, $G$ is assumed to satisfy

$$G_B = \frac{\partial G}{\partial B} > 0, G_{BB} = \frac{\partial^2 G}{\partial B^2} \leq 0, G_Z = \frac{\partial G}{\partial Z} < 0.$$

Thus, biodiversity growth increases with existing ecological richness at a non-increasing rate and decreases with cumulative harvesting pressure. Boundary behavior is imposed so that biodiversity growth weakens near ecological saturation or excessive cumulative harvesting pressure, for example as $B(t) \to \bar{B}$ or $Z(t) \to \bar{Z}$, where $\bar{B}$ and $\bar{Z}$ denote ecological threshold levels.

Disturbance ecology further recognizes that biodiversity may experience abrupt losses from fires, windthrow, pest outbreaks, pathogen incursions, or other extreme events (Turner 2010; Johnstone et al. 2016). To motivate a tractable representation of such pulse disturbances, consider

$$dB_t = G(B_{t^-}, Z_{t^-})dt - B_{t^-}\ell_t dN_t, \tag{5}$$

where $N_t$ is a Poisson counting process with intensity $\varpi > 0$, distinct from the discount rate $\rho$, and $\ell_t \in [0,1]$ is a random proportional biodiversity-loss factor. The notation $t^-$ denotes the pre-jump state. Since $\ell_t \in [0,1]$, the post-disturbance biodiversity stock remains nonnegative. This pulse-event representation is consistent with disturbance-based ecological modeling and complements continuous-noise formulations such as Lande (1993).

This compound Poisson representation is used to translate intermittent disturbance risk into an expected-drift biodiversity-loss term within the deterministic finite-horizon control framework. Let

$$\bar{\ell} = \mathbb{E}[\ell_t]. \tag{6a}$$

where $\bar{\ell}$ is the finite mean proportional biodiversity loss per disturbance event. Let $\mathcal{F}_{t^-}$ denote the information set available immediately before time $t$, including the pre-jump ecological state and disturbance history but excluding the realization of a possible jump at $t$. We assume that $\ell_t$ is independent of both the Poisson increment $dN_t$ and the pre-jump information set $\mathcal{F}_{t^-}$. Conditional on $\mathcal{F}_{t^-}$,

$$\mathbb{E}[dN_t|\mathcal{F}_{t^-}] = \varpi dt. \tag{6b}$$

Taking conditional expectations in Equation (5) gives

$$\frac{\mathbb{E}[dB_t|\mathcal{F}_{t^-}]}{dt} = G(B_{t^-}, Z_{t^-}) - \varpi B_{t^-}\bar{\ell} \tag{6c}$$



19397445, 2026, 3, Downloaded from https://onlinelibrary.wiley.com/doi/10.1111/nrm.70037 by CochraneItalia, Wiley Online Library on [04/07/2026]. See the Terms and Conditions (https://onlinelibrary.wiley.com/terms-and-conditions) on Wiley Online Library for rules of use; OA articles are governed by the applicable Creative Commons License

Dropping pre-jump notation in the deterministic benchmark yields

$$\dot{B}(t) = G(B(t), Z(t)) - \varpi B(t)\overline{\ell}. \tag{6d}$$

For the baseline deterministic simulations, the expected proportional loss is evaluated at a reference biodiversity level $B_{ref}$. Define

$$\kappa \equiv B_{ref}\,\overline{\ell}, \tag{6e}$$

where $\kappa$ is the calibrated expected biodiversity loss per disturbance arrival. The biodiversity equation becomes

$$\dot{B}(t) = G(B(t), Z(t)) - \varpi\kappa. \tag{6}$$

This reduction preserves the disturbance interpretation of $\varpi\kappa$ while keeping the subsequent finite-horizon control systems deterministic. If disturbance frequency or expected severity depends on an exogenous climate variable, such as a temperature anomaly $T_t$, the same structure can accommodate $\varpi = \varpi(T_t)$ or $\overline{\ell} = \overline{\ell}(T_t)$. The baseline simulations use constant $\varpi\kappa$.

For biodiversity growth, we use the general regeneration–damage specification

$$G(B(t), Z(t)) = gB(t)^a - \delta Z(t)^b, g, \delta > 0, 0 < a \leq 1, b \geq 1, \tag{7}$$

Here $g$ is the biodiversity-regeneration parameter, $\delta$ measures the adverse effect of cumulative harvesting pressure, $a$ governs the curvature of biodiversity recovery, and $b$ governs the curvature of cumulative-pressure damage. Substituting Equation (7) into Equation (6) gives

$$\dot{B}(t) = gB(t)^a - \delta Z(t)^b - \varpi\kappa. \tag{8}$$

Appendix B examines robustness to this nonlinear biodiversity specification. In the baseline simulations, we use the linear benchmark $a = b = 1$:

$$\dot{B}(t) = gB(t) - \delta Z(t) - \varpi\kappa. \tag{9}$$

The steady states and local properties of the deterministic ecological subsystem in Equations (2), (9), and (10) are summarized in Appendix A.

Cumulative harvesting pressure evolves according to

$$\dot{Z}(t) = \sum_{i=1}^{n} u_i(t) - \gamma Z(t), \gamma > 0, \tag{10}$$

where $\gamma$ is the decay rate of historical harvesting effects.

Each harvester $i$ maximizes discounted profit,

$$\pi_i = \max_{u_i(.)\in\mathcal{U}_i} \int_0^T e^{-\rho t}[p(t)u_i(t) - C_i(u_i(t))]dt, \tag{11}$$

where $p(t)$ is the exogenous biomass price, $C_i(.)$ is a convex harvesting-cost function, and $\rho > 0$ is the discount rate. For each harvester $i$, the admissible-control set is

$$\mathcal{U}_i = \Big\{u_i \in L^2([0, T]; \mathbb{R}_+) : \textit{the induced state trajectory satisfies } (x(t), B(t), Z(t)) \in \mathbb{R}^3_+ \quad \forall\, t \in \Big[0, T\Big]\Big\}. \tag{12}$$

Initial states are fixed:

$$(x(0), \quad B(0), \quad Z(0)) = (x_0, B_0, Z_0). \tag{13}$$

Fixed-terminal regimes impose

$$(x(T), \quad B(T), Z(T)) = (x_T, B_T, Z_T). \tag{14}$$

whereas free-terminal regimes impose the current-value transversality conditions

$$\lambda(T) = \mu(T) = \nu(T) = 0. \tag{15}$$

Here $\lambda(t)$, $\mu(t)$, and $\nu(t)$ are the current-value costates associated with biomass $x(t)$, biodiversity $B(t)$, and cumulative harvesting pressure $Z(t)$, respectively. The finite-horizon optimality conditions follow from Pontryagin's Maximum Principle (PMP) with endpoint constraints (Seierstad and Sydsæter 1987; Bryson 2018).

In the open-loop Nash regime, agent $i$ chooses $u_i(t)$ while taking the other agents' controls $\overline{u}_j(t)$, $j \neq i$, as given. The current-value Hamiltonian[2] for harvester $i$ is

$$\begin{aligned} H_i = {} & p(t)u_i(t) - C_i(u_i(t)) + \lambda_i(t)\Big[r(B(t))x(t)\left(1 - \frac{x(t)}{K}\right) - u_i(t) - \sum_{j\neq i}\overline{u}_j(t)\Big] \\ & + \mu_i(t)[gB(t) - \delta Z(t) - \varpi\kappa] \\ & + \nu_i(t)\Big[u_i(t) + \sum_{j\neq i}\overline{u}_j(t) - \gamma Z(t)\Big] + s_i(t)u_i(t) \end{aligned} \tag{16}$$

where $s_i(t) \geq 0$ is the Kuhn–Tucker multiplier for $u_i(t) \geq 0$ and $\lambda_i(t)$, $\mu_i(t)$, $\nu_i(t)$ are the agent-specific current-value costates. The stationarity and complementarity conditions are

$$\frac{\partial H_i}{\partial u_i} = p(t) - C_i'(u_i(t)) - \lambda_i(t) + \nu_i(t) + s_i(t) = 0, \tag{17}$$

$$u_i(t) \geq 0, \quad s_i(t) \geq 0, s_i(t)u_i(t) = 0. \tag{18}$$

With quadratic harvesting costs,

$$C_i(u_i(t)) = \frac{\alpha_{C_i}}{2}(u_i(t))^2, \alpha_{C_i} > 0, \tag{19}$$



19397445, 2026, 3, Downloaded from https://onlinelibrary.wiley.com/doi/10.1111/nrm.70037 by CochraneItalia, Wiley Online Library on [04/07/2026]. See the Terms and Conditions (https://onlinelibrary.wiley.com/terms-and-conditions) on Wiley Online Library for rules of use; OA articles are governed by the applicable Creative Commons License

where $\alpha_{C_i}$ is the cost-curvature parameter, the projected harvesting rule is

$$u_i^*(t) = \max\left\{0, \frac{p(t) - \lambda_i(t) + \nu_i(t)}{\alpha_{C_i}}\right\}. \tag{20}$$

Under symmetry, $\alpha_{C_i} = \alpha_C$ for all $i$, $u_i^*(t) = u^*(t)$, and aggregate harvesting is $U^*(t) = nu^*(t)$. The symmetric open-loop Nash system is

$$\begin{cases} \dot{x}(t) = r(B(t))x(t)\left(1 - \dfrac{x(t)}{K}\right) - nu^*(t) \\ \dot{B}(t) = gB(t) - \delta Z(t) - \varpi\kappa \\ \dot{Z}(t) = nu^*(t) - \gamma Z(t) \\ \dot{\lambda}(t) = \rho\lambda(t) - \lambda(t)r(B(t))\left(1 - \dfrac{2x(t)}{K}\right) \\ \dot{\mu}(t) = \rho\mu(t) - \left[\lambda(t)r'(B(t))x(t)\left(1 - \dfrac{x(t)}{K}\right) + g\mu(t)\right] \\ \dot{\nu}(t) = \rho\nu(t) - [-\delta\mu(t) - \gamma\nu(t)] \end{cases} \tag{21}$$

The projected control satisfies

$$u^*(t) = 0 \text{ if } p(t) - \lambda(t) + \nu(t) \le 0,$$

and otherwise

$$u^*(t) = \frac{p(t) - \lambda(t) + \nu(t)}{\alpha_C}. \tag{22}$$

Equations (21–22), together with the relevant initial and terminal conditions, define the symmetric open-loop Nash benchmark.

We next consider the cooperative governance regime. In this case, a regulator chooses the full harvesting profile

$$\mathbf{u}(t) = (u_1(t), \cdots, u_n(t)), \tag{23}$$

to maximize total discounted welfare. The planner's admissible-control set is

$$\mathcal{U} = \left\{\mathbf{u} \in L^2\left([0, T]; \mathbb{R}_+^n\right) : \textit{the induced state trajectory satisfies } (x(t), B(t), \quad Z(t)) \in \mathbb{R}_+^3 \quad \forall\, t \in \left[0, T\right]\right\}. \tag{24}$$

The cooperative objective is

$$W = \max_{\mathbf{u}(.)\in\mathcal{U}} \int_0^T e^{-\rho t}\left[\sum_{i=1}^n (p(t)u_i(t) - C_i(u_i(t))) + V_1(B(t)) + V_2(x(t))\right]dt, \tag{25}$$

where $V_1(B(t))$ is the social value of biodiversity and $V_2(x(t))$ is the social value of standing biomass. Both functions are assumed increasing and concave, representing positive but diminishing marginal social valuation.

The regulator's current-value Hamiltonian is

$$\begin{aligned} H^R = {} & \sum_{i=1}^n [p(t)u_i(t) - C_i(u_i(t))] + V_1(B(t)) \\ & + V_2(x(t)) + \lambda(t)\left[r(B(t))x(t)\left(1 - \frac{x(t)}{K}\right) - \sum_{i=1}^n u_i(t)\right] + \mu(t)[gB(t) - \delta Z(t) - \varpi\kappa] \\ & + \nu(t)\left[\sum_{i=1}^n u_i(t) - \gamma Z(t)\right] + \sum_{i=1}^n s_i(t)u_i(t) \end{aligned} \tag{26}$$

For each $i$, the stationarity and complementarity conditions are

$$\frac{\partial H^R}{\partial u_i} = p(t) - C_i'(u_i(t)) - \lambda(t) + \nu(t) + s_i(t) = 0, \tag{27}$$

$$u_i(t) \ge 0, s_i(t) \ge 0, s_i(t)u_i(t) = 0. \tag{28}$$

With quadratic costs,

$$u_i^*(t) = \max\left\{0, \frac{p(t) - \lambda(t) + \nu(t)}{\alpha_{C_i}}\right\}. \tag{29}$$

Under the symmetry convention introduced in the Nash case, the cooperative controls satisfy $u_i^*(t) = u^*(t)$ for all $i$, and aggregate harvesting is $U^*(t) = nu^*(t)$. The cooperative forward–backward system is

$$\begin{cases} \dot{x}(t) = r(B(t))x(t)\left(1 - \dfrac{x(t)}{K}\right) - nu^*(t) \\ \dot{B}(t) = gB(t) - \delta Z(t) - \varpi\kappa \\ \dot{Z}(t) = nu^*(t) - \gamma Z(t) \\ \dot{\lambda}(t) = \rho\lambda(t) - \left[V_2'(x(t)) + \lambda(t)r(B(t))\left(1 - \dfrac{2x(t)}{K}\right)\right] \\ \dot{\mu}(t) = \rho\mu(t) - \left[V_1'(B(t)) + \lambda(t)r'(B(t))x(t)\left(1 - \dfrac{x(t)}{K}\right) + g\mu(t)\right] \\ \dot{\nu}(t) = \rho\nu(t) - [-\delta\mu(t) - \gamma\nu(t)] \end{cases} \tag{30}$$

The open-loop Nash system in Equation (21) and the cooperative system in Equation (30) are deterministic finite-horizon Pontryagin systems. Disturbance exposure enters these systems only through the expected-loss term $\varpi\kappa$. Accordingly, the numerical analysis should be interpreted as a deterministic finite-horizon comparison of governance regimes, with



19397445, 2026, 3, Downloaded from https://onlinelibrary.wiley.com/doi/10.1111/nrm.70037 by CochraneItalia, Wiley Online Library on [04/07/2026]. See the Terms and Conditions (https://onlinelibrary.wiley.com/terms-and-conditions) on Wiley Online Library for rules of use; OA articles are governed by the applicable Creative Commons License

disturbance exposure incorporated through the expected biodiversity-loss term $\varpi\kappa$.

The systems are solved on $[0, T]$ using a shooting-based boundary-value method. Initial states are fixed, and initial costates are adjusted to satisfy either the free-terminal transversality conditions or the fixed terminal state constraints. The numerical implementation uses stiffness-aware integration with high working precision, following standard numerical practice for nonlinear dynamic systems and boundary-value problems (Kushner 1990; Seyedi 2010; Seyedi et al. 2018; Xepapadeas 2022). Sensitivity analysis over $\delta, g, \rho, \gamma, p$ and $\varpi\kappa$ is reported in the Supporting Information S1.

Under strictly positive parameters, interior initial states, and admissible controls preserving the feasible ecological domain, the state–costate right-hand sides are continuous and locally Lipschitz. Standard existence and continuous-dependence results therefore apply to the associated initial-value formulation over the finite horizon (Hale and Koçak 1991; Teschl 2012). Feasibility within the ecological domain is consistent with standard viability arguments for constrained dynamics (Nagumo 1942; Lee and Haddad 2021). Local stability and numerical behavior are assessed within the calibrated deterministic benchmark, using standard tools for nonlinear systems and stiff integration (Khalil 2002; Hairer et al. 1993; Hairer and Wanner 1996; Stoer and Bulirsch 2002). Accordingly, the policy interpretation is restricted to comparative implications within this deterministic finite-horizon framework: the analysis compares how governance regime and endpoint design shape harvesting incentives, biodiversity trajectories, biomass conservation, and welfare outcomes.

## 4 | Results

This section reports numerical solutions of the deterministic finite-horizon Pontryagin systems derived in Section 3. The systems are solved over $t \in [0, T]$, with $T = 20$, for three governance regimes: the symmetric open-loop Nash equilibrium with free terminal states, the cooperative regulator with fixed terminal state constraints, and the cooperative regulator with free terminal states. The open-loop Nash benchmark is obtained from Equation (21), together with the projected control rule in Equations (20–22). The cooperative regulator problem is obtained from Equation (30), under either fixed-terminal state constraints or free-terminal transversality conditions.

Throughout the baseline simulations, the biodiversity dynamics follow the linear deterministic benchmark in Equation (9), where disturbance exposure enters only through the expected-loss term $\varpi\kappa$. Baseline parameters, initial conditions, and numerical settings are held common across regimes, except for objective structure and endpoint conditions, as reported in Supporting Information S2. The coupled forward–backward systems are solved using a shooting-based boundary-value procedure with stiffness-adaptive integration and high working precision, following standard numerical practice for nonlinear dynamic systems and boundary-value problems (Kushner 1990; Seyedi 2010; Seyedi et al. 2018; Xepapadeas 2022). Numerical reliability is assessed through boundary-residual diagnostics, mesh refinement, and stability under tighter solver tolerances, as described in Supporting Information S2.

### 4.1 | State Trajectories

Figure 1 summarizes the baseline trajectories of the state variables $x(t)$, $B(t)$, and $Z(t)$, together with the associated costates, generated by the deterministic system in Equations (2), (9), and (10), with $\varpi\kappa = 10^{-4}$. Biomass $x(t)$ declines in all regimes, but the rate of decline differs across governance structures. The cooperative free-endpoint regime, Reg-Free, maintains the highest terminal biomass, approximately $x(20) \approx 410$. The OLNE-Free benchmark exhibits the steepest biomass decline, reaching approximately $x(20) \approx 385$. The cooperative fixed-endpoint regime, Reg-Fixed, converges to its prescribed terminal target $x(20) \approx 400$, producing an intermediate terminal biomass outcome.

Biodiversity $B(t)$ increases in all three regimes under the baseline calibration. This pattern reflects the positive regenerative component in the benchmark biodiversity equation, together with moderate cumulative-pressure and expected-loss effects over the finite horizon. Reg-Free generates the strongest biodiversity recovery, with $B(20) \approx 350$. OLNE-Free is intermediate, with $B(20) \approx 230$, while Reg-Fixed reaches the imposed terminal target $B(20) \approx 150$. These rankings are consistent with the productivity feedback in Equation (3): higher biodiversity raises $r(B(t))$, which in turn strengthens the regenerative component of biomass growth in Equation (2).

Cumulative harvesting pressure $Z(t)$ shows the clearest regime separation. Under OLNE-Free, $Z(t)$ rises rapidly and then levels off near $Z(20) \approx 20$. Under Reg-Free, cumulative harvesting pressure increases more gradually and reaches a slightly lower terminal level, approximately $Z(20) \in [19, 19.5]$. Reg-Fixed displays a distinct inverted-U pattern: cumulative harvesting pressure rises early, reaches approximately $Z \approx 20$ around the middle of the horizon, and then declines toward the imposed terminal target $Z(20) \approx 10$. This pattern reflects the boundary adjustment required by the fixed-endpoint formulation.

### 4.2 | Harvest Controls

Figure 2a reports the implied symmetric harvest intensity $u^*(t)$. Under the quadratic harvesting-cost specification, OLNE-Free produces an almost constant harvest profile, approximately $u^*(t) \approx 0.4$. This reflects the near time-invariance of the shadow-value wedge $p(t) - \lambda(t) + \nu(t)$ along the baseline OLNE-Free solution.

Reg-Fixed begins with substantially higher extraction, approximately $u^*(0) \approx 0.7$, and then reduces harvesting over time to satisfy the terminal state constraints. By contrast, Reg-Free begins with low extraction, approximately $u^*(0) \approx 0.1$, and gradually increases toward the OLNE-Free level by the end of the horizon. This pattern is consistent with a cooperative planner internalizing the productivity value of biodiversity early in the horizon while allowing terminal states to adjust endogenously under free-endpoint conditions.



19397445, 2026, 3, Downloaded from https://onlinelibrary.wiley.com/doi/10.1111/nrm.70037 by CochraneItalia, Wiley Online Library on [04/07/2026]. See the Terms and Conditions (https://onlinelibrary.wiley.com/terms-and-conditions) on Wiley Online Library for rules of use; OA articles are governed by the applicable Creative Commons License

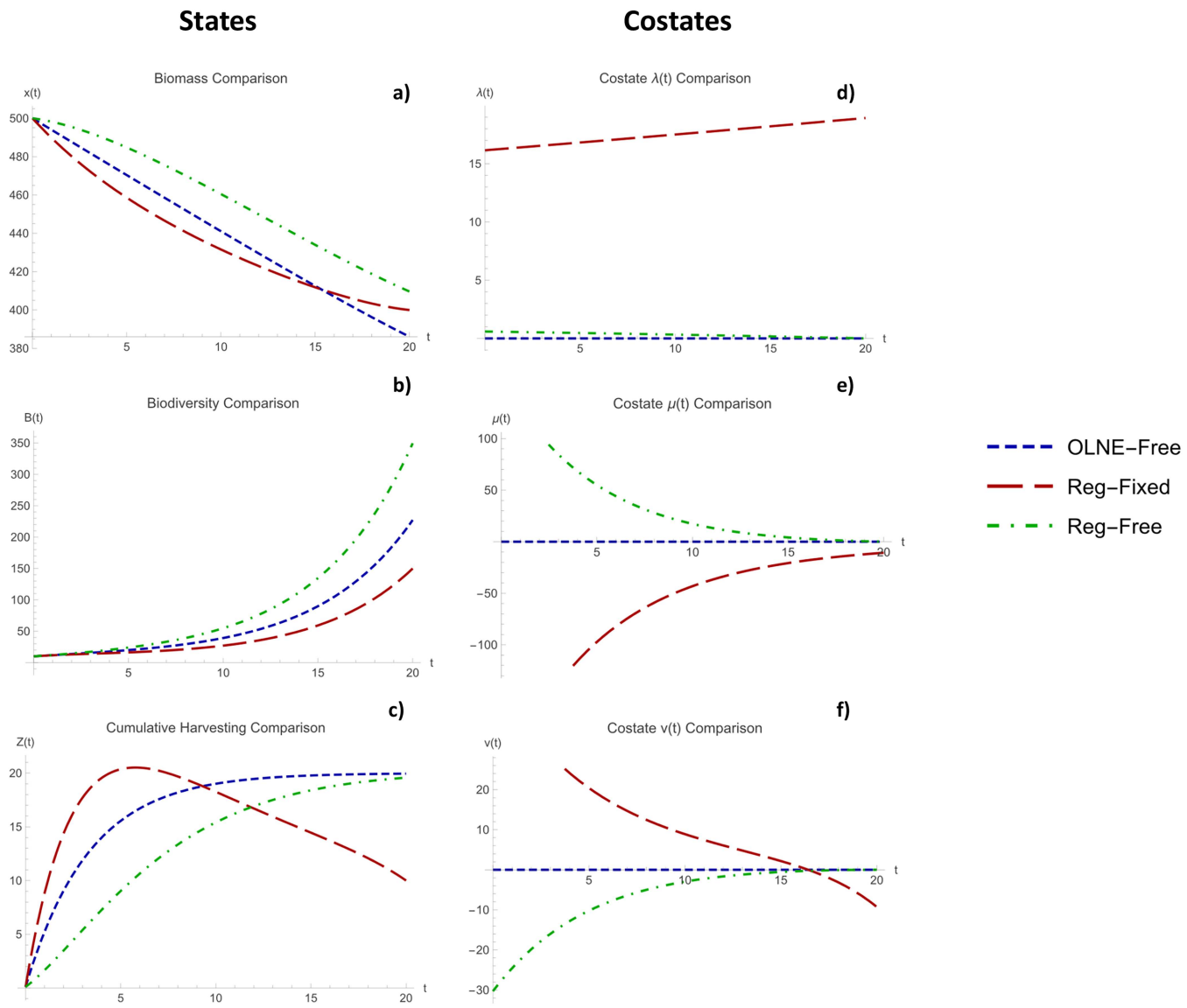


**FIGURE 1** | Temporal dynamics of ecological states and shadow prices under alternative governance regimes. Time evolution of state variables and current-value costates under three governance regimes: noncooperative open-loop Nash with free terminal states (OLNE-Free), cooperative regulation with fixed terminal targets (Reg-Fixed), and cooperative regulation with free terminal states (Reg-Free). Panels (a–c) show the trajectories of biomass $x(t)$, biodiversity $B(t)$, and cumulative harvesting pressure $Z(t)$, respectively. Panels (d–f) show the corresponding shadow prices: the biomass costate $\lambda(t)$, biodiversity costate $\mu(t)$, and cumulative harvesting pressure costate $\nu(t)$. Simulations use the following parameters: $g = 0.2, \gamma = 0.3, A = 2 \times 10^{-5}, \zeta = 1, K = 1000, \rho = 0.01, p = 40, n = 15, \delta = 0.1, \alpha_C = 100,$ with initial conditions $(x_0, B_0, Z_0) = (500,10,0.1)$. Fixed-endpoint simulations impose terminal state constraints $(x_T, B_T, Z_T) = (400,150,10)$ at horizon $T = 20$.

### 4.3 | Costate Dynamics

Figure 1d–f reports the costate variables $\lambda(t)$, $\mu(t)$, and $\nu(t)$, associated respectively with biomass, biodiversity, and cumulative harvesting pressure. The biomass shadow value $\lambda(t)$ is substantially larger in Reg-Fixed than in the other regimes, remaining roughly between 16 and 18 over the horizon. This reflects the scarcity value induced by binding terminal stock requirements. In OLNE-Free and Reg-Free, $\lambda(t)$ remains close to zero on the plotted scale, although Reg-Free lies slightly above OLNE-Free, consistent with cooperative internalization of ecological feedbacks.

The biodiversity shadow value $\mu(t)$ also differs across regimes. In Reg-Free, $\mu(t)$ starts positive and declines toward zero as the terminal date approaches, consistent with the free-endpoint transversality condition. In Reg-Fixed, $\mu(t)$ is initially negative and then moves toward zero as the trajectory adjusts to the terminal biodiversity target. In OLNE-Free, $\mu(t)$ remains close to zero, indicating limited private valuation of biodiversity as productive ecological capital relative to the cooperative regimes.

The pressure shadow value $\nu(t)$ reflects the intertemporal value of cumulative harvesting pressure. Reg-Fixed displays a sign change over the horizon, moving from positive values early in the simulation to negative values near the terminal date. This is consistent with the terminal correction observed in $Z(t)$. Reg-Free starts negative and converges smoothly toward zero, consistent with the free-terminal transversality condition.



19397445, 2026, 3, Downloaded from https://onlinelibrary.wiley.com/doi/10.1111/nrm.70037 by CochraneItalia, Wiley Online Library on [04/07/2026]. See the Terms and Conditions (https://onlinelibrary.wiley.com/terms-and-conditions) on Wiley Online Library for rules of use; OA articles are governed by the applicable Creative Commons License

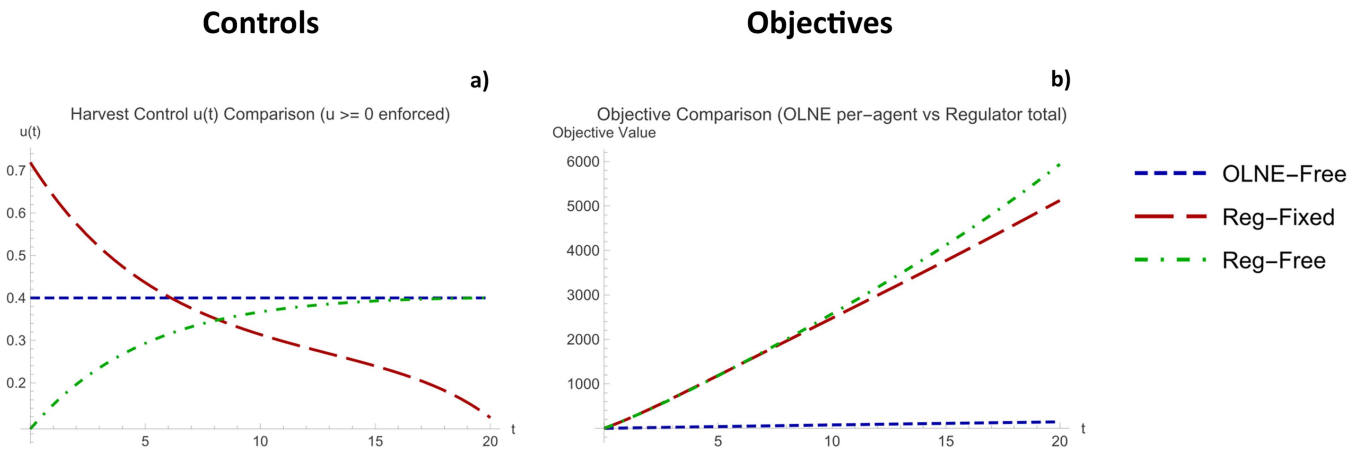


**FIGURE 2** | Optimal harvest strategies and cumulative objective values under alternative governance regimes. Panel a shows the time path of the symmetric optimal harvest intensity $u^*(t)$ for each regime. Panel b displays the corresponding cumulative present-value objective aggregated up to time $t$. All simulations use the same baseline calibration as in Figure 1, with regime-specific endpoint conditions and consistent linestyle conventions applied across panels.

### 4.4 | Objective Values

Figure 2b reports cumulative objective values under the objective definitions used for each regime. The cooperative objective paths are higher than the plotted OLNE benchmark objective path, and Reg-Free attains the highest cumulative regulator objective in the baseline simulation. This comparison should be interpreted within the model's specified objective structure: the cooperative regimes include the regulator's valuation of biomass and biodiversity, whereas OLNE-Free represents decentralized harvesting incentives. The difference between Reg-Free and Reg-Fixed reflects the role of endpoint design. Fixed-terminal constraints impose prescribed ecological targets but restrict adjustment, while the free-endpoint cooperative regime allows the planner to internalize biodiversity–productivity feedbacks without being constrained to meet prescribed terminal state values.

Appendix A provides analytical context for these numerical paths by characterizing steady states and local properties of the deterministic ecological subsystem under a constant-harvest benchmark. That analysis yields the standard high- and low-biomass branches of harvested logistic growth and shows mean reversion of cumulative harvesting pressure when $\gamma > 0$. The simulated Pontryagin trajectories should therefore be interpreted as controlled finite-horizon paths shaped jointly by the projected harvesting rule, the costate dynamics, and the endpoint conditions. This interpretation is consistent with the terminal adjustment in Reg-Fixed and the smoother trajectories under Reg-Free.

### 4.5 | Sensitivity Analysis

Supporting Information S1: Figure 1 reports local first-order sensitivities of the state trajectories $y(t) \in \{x(t), B(t)\}$, with respect to selected ecological and economic parameters, $\theta \in \{\delta, g, \rho, \gamma, p, \varpi\kappa\}$. Following the protocol described in Supporting Information S1, each parameter perturbation is evaluated by re-solving the corresponding boundary-value problem under the same governance regime and endpoint design. This re-solve-and-difference procedure captures not only direct parameter effects in the state equations but also induced changes in costates, controls, and boundary matching.

The sensitivity paths are summarized in Supporting Information S1 using two scalar measures: peak absolute sensitivity and time-integrated absolute sensitivity. The results indicate three local patterns around the calibrated baseline. First, OLNE-Free displays relatively large responses for several ecological drivers, especially $\delta$ and $\varpi\kappa$, suggesting greater local exposure of the noncooperative benchmark to cumulative-pressure and expected-loss parameters. Second, Reg-Fixed exhibits non-monotone sensitivity profiles with stronger terminal effects, reflecting the fixed endpoint constraints. Third, Reg-Free produces smoother sensitivity paths, consistent with the absence of prescribed terminal state targets. These results should be interpreted as local comparative statics around the calibrated deterministic benchmark, not as global robustness claims over the full parameter space.

### 4.6 | Policy Implications

The numerical results indicate a persistent difference between decentralized and cooperative harvesting incentives within the deterministic finite-horizon model. Under OLNE-Free, private harvesters do not internalize the full biodiversity–productivity feedback embedded in $r(B(t))$. Consequently, biomass declines more rapidly and cumulative harvesting pressure builds up more strongly than in the cooperative regimes. The costate trajectories provide the corresponding shadow-value interpretation: the cooperative regimes assign greater marginal value to ecological states, especially when terminal ecological targets are imposed.

A useful model-based diagnostic is the shadow-value wedge between cooperative and noncooperative biomass valuation. Within the model, one can define $\tau(t) = \lambda_{Reg}(t) - \lambda_{OLNE}(t)$, which measures the difference between the cooperative and decentralized marginal valuations of standing biomass. This wedge can be interpreted as an indicative per-unit harvest



19397445, 2026, 3, Downloaded from https://onlinelibrary.wiley.com/doi/10.1111/nrm.70037 by CochraneItalia, Wiley Online Library on [04/07/2026]. See the Terms and Conditions (https://onlinelibrary.wiley.com/terms-and-conditions) on Wiley Online Library for rules of use; OA articles are governed by the applicable Creative Commons License

correction implied by the necessary conditions. In Reg-Fixed, the wedge is large because the fixed terminal stock requirements generate high biomass shadow values. In Reg-Free, the wedge is smaller and smoother, reflecting more gradual intertemporal adjustment under free terminal states.

This interpretation should be read as a model-based implication rather than a complete policy design. The results suggest that instruments linked to ecological shadow values could help align private harvesting incentives with cooperative ecological valuation. Depending on implementation constraints, such instruments could take the form of harvest charges, conservation subsidies, payments for ecosystem services, or performance-based mechanisms. The model does not determine a fully specified institutional instrument; rather, it identifies the direction and timing of incentive adjustments implied by the optimality conditions.

Figure 2a illustrates how these incentive differences translate into harvest paths. OLNE-Free maintains a nearly constant harvest level, Reg-Fixed reduces harvest over time to satisfy terminal constraints, and Reg-Free follows a smoother adaptive path. Figure 2b shows that the cooperative objective paths exceed the plotted OLNE-Free benchmark objective path in the calibrated baseline, with Reg-Free achieving the highest cumulative regulator value. This pattern reflects the value of internalizing biodiversity's contribution to productivity while retaining flexibility over terminal ecological states.

Supporting Information S1: Figure 1 further suggests that model-implied incentive corrections may vary with ecological conditions. In particular, the local sensitivity analysis indicates stronger noncooperative exposure to cumulative-pressure damage and expected disturbance losses, while cooperative regimes display smoother or more endpoint-specific responses. These implications remain limited to the comparative mechanisms identified by the deterministic finite-horizon benchmark.

## 5 | Discussion and Final Remarks

The present analysis examines the dynamic interaction among biomass, biodiversity, and harvesting in a spatially homogeneous forest ecosystem. The model is deliberately formulated as a deterministic finite-horizon control framework in which biodiversity affects biomass productivity and cumulative harvesting pressure creates an ecological memory channel. Within this setting, the numerical results show how governance structure and endpoint design shape ecological trajectories, harvesting incentives, and objective values. This framing is consistent with the bioeconomic tradition of using structured dynamic models to clarify mechanisms linking resource use, ecological stocks, and intertemporal incentives (Clark 2010).

A central implication of the analysis is that biodiversity-dependent productivity materially affects the comparison between decentralized and cooperative governance. The specification $r(B)$ links biodiversity to biomass regeneration, reflecting ecological evidence that biodiversity can enhance ecosystem functioning and productivity, often in nonlinear ways (Tilman et al. 1996; Cardinale et al. 2012). In the calibrated simulations, cooperative regimes generate higher biomass and biodiversity paths than the open-loop Nash benchmark. This occurs because the cooperative planner internalizes the contribution of biodiversity to future productivity, whereas decentralized harvesters respond primarily to their own harvesting returns. The resulting divergence is not merely a difference in terminal stocks; it reflects a difference in the intertemporal valuation of ecological capital.

The costate trajectories clarify this mechanism. The shadow values associated with biomass, biodiversity, and cumulative harvesting pressure reveal how each governance regime values ecological states over the finite horizon. In particular, the cooperative regimes assign higher marginal value to ecological stocks, especially when terminal targets are imposed. The open-loop Nash benchmark, by contrast, exhibits weaker private valuation of biodiversity as productive ecological capital. This valuation gap provides a model-based explanation for the differences in harvest paths and ecological outcomes. It also connects the analysis to broader work emphasizing the importance of incorporating ecosystem values into economic decision-making (Barbier 2011; Costanza et al. 2014).

The policy implications should be interpreted with appropriate restraint. The model does not derive or evaluate a complete policy instrument. Instead, it identifies a shadow-value wedge that provides an indicative measure of how private harvesting incentives differ from cooperative ecological valuation. This is consistent with classical resource-taxation logic and optimal-control reasoning (Reed 1979), while recognizing that implementation of any Pigouvian-type instrument would require additional institutional assumptions. In this sense, the shadow-value wedge provides a diagnostic for the timing and direction of potential incentive adjustments.

The sensitivity results reinforce the importance of interpreting the numerical findings as local comparative statics around the calibrated deterministic benchmark. Supporting Information S1: Figure 1 shows that the noncooperative benchmark is more responsive to selected ecological drivers, especially the cumulative-pressure parameter $\delta$ and the expected disturbance-loss term $\varpi\kappa$. Cooperative designs generate smoother and generally more attenuated sensitivity profiles, although fixed endpoints introduce stronger terminal adjustments. These patterns indicate that governance regime and endpoint design affect not only baseline trajectories but also local responsiveness to parameter changes. They should not, however, be interpreted as global robustness results over the full parameter space. This restrained interpretation is consistent with the broader concern that unpriced natural capital may be vulnerable to ecological shocks and intertemporal undervaluation (Dasgupta 2021).

Endpoint design is also central to the results. Fixed terminal constraints provide explicit ecological targets, but they can induce boundary adjustments near the end of the planning horizon. This is visible in the Reg-Fixed trajectory for cumulative harvesting pressure and in the associated costate dynamics. Free-terminal cooperative governance allows smoother adjustment because terminal states are determined endogenously through transversality conditions. This distinction is consistent with standard finite-horizon optimal-control theory, where



19397445, 2026, 3, Downloaded from https://onlinelibrary.wiley.com/doi/10.1111/nrm.70037 by CochraneItalia, Wiley Online Library on [04/07/2026]. See the Terms and Conditions (https://onlinelibrary.wiley.com/terms-and-conditions) on Wiley Online Library for rules of use; OA articles are governed by the applicable Creative Commons License

endpoint restrictions shape both state trajectories and shadow prices (Seierstad and Sydsæter 1987). In this sense, the comparison between fixed and free endpoints highlights a trade-off between target-based sustainability constraints and adaptive flexibility.

The institutional interpretation of these results should also remain tied to the formal model. The findings support the view that incentive-compatible governance may improve outcomes when ecological feedbacks are not internalized by private harvesters. This is broadly consistent with work on polycentric and context-sensitive environmental governance, where local adaptation, monitoring, and institutional flexibility are important for responding to ecological feedbacks (Ostrom 2009; Arjomandi A et al. 2022; Arjomandi A et al. 2024; Arjomandi A et al. 2025). However, the model abstracts from many institutional details, including enforcement capacity, property-rights heterogeneity, information constraints, and political feasibility. Therefore, the results should be read as identifying mechanisms rather than prescribing a complete governance architecture.

The disturbance component should be interpreted in the same restrained way. The model uses a disturbance-motivated expected-loss term, $\varpi\kappa$, within a deterministic control system. It does not solve a stochastic-control problem or simulate stochastic sample paths. Nevertheless, the expected-loss term provides a tractable way to incorporate average disturbance exposure into biodiversity dynamics. This is relevant because ecological systems may be affected by disturbance processes, environmental variability, and climate-related stressors (Tilman et al. 2006; Hong et al. 2022; Oliveira et al. 2022). The present framework captures only the mean-loss channel and should therefore be viewed as a deterministic benchmark rather than a full treatment of disturbance risk.

From an implementation perspective, the shadow-value interpretation suggests that practical instruments would require ecological monitoring, transparent measurement, and institutional capacity. Advances in ecological data collection and monitoring can support more adaptive regulatory approaches (Bush et al. 2017). Yet direct implementation of dynamic harvest charges may be difficult when monitoring is costly, resource use is hard to attribute, or ecological responsibilities are contested (Tilman et al. 2006; Ostrom 2009; Hong et al. 2022; Oliveira et al. 2022; Arjomandi A et al. 2022; Arjomandi A et al. 2024). In such settings, complementary instruments such as payments for ecosystem services, conservation subsidies, or ecological performance bonds may provide more feasible ways to approximate cooperative incentives. These mechanisms can reward conservation or reduced extraction rather than relying exclusively on enforceable fees, making them relevant where enforcement capacity or property rights are incomplete (Baumgärtner and Quaas 2010; Farley and Costanza 2010; Wunder 2015).

Several extensions would strengthen the framework. First, future work could allow disturbance exposure to depend endogenously on ecological states, so that degraded biomass or biodiversity increases vulnerability to future losses. Second, the model could incorporate climate stressors, spatial fragmentation, and landscape heterogeneity, relaxing the spatial homogeneity assumption. Third, richer ecological nonlinearities such as Allee effects, trophic interactions, threshold dynamics, and landscape connectivity could be introduced to study longer-run resilience and regime shifts (Scheffer et al. 2001; Rockström et al. 2009; Dasgupta 2021). Finally, future research could develop a genuinely stochastic-control or stochastic-simulation version of the model to examine the distribution of ecological paths and the performance of feedback policies under realized disturbances.

In summary, the analysis highlights the importance of incorporating biodiversity and ecological memory into dynamic bioeconomic decision-making. Within the deterministic finite-horizon benchmark studied here, cooperative governance generates more favorable ecological trajectories and objective-value outcomes relative to the noncooperative benchmark by internalizing biodiversity's contribution to productivity and by accounting for cumulative harvesting pressure. The results do not prescribe a specific policy instrument, but they provide a formal basis for understanding how shadow-value wedges may inform incentive-compatible conservation mechanisms. This perspective is relevant to broader debates on forest conservation, payments for ecosystem services, REDD+, and biodiversity-oriented policy frameworks, including those associated with IPBES and related initiatives (Clark 2010; Bongaarts 2019; Wunder 2005). Recent discussions of conservation-linked financial instruments, including "Amazonia" bonds, further illustrate the growing policy interest in linking financial incentives to measurable conservation outcomes (Reuters 2024). Although such instruments are not explicitly modeled here, the shadow-value logic developed in this study provides a structured way to think about how ecological valuation could inform their design in strategic forest-management settings.

## Author Contributions

**Seyedalireza Seyedi:** conceptualization, methodology, investigation, formal analysis, validation, visualization, writing – original draft, writing – review and editing. **Elettra Agliardi:** conceptualization, methodology, investigation, validation, formal analysis, supervision, project administration, writing – original draft, writing – review and editing, visualization. **Anastasios Xepapadeas:** conceptualization, methodology, investigation, validation, visualization, writing – original draft, writing – review and editing, supervision, project administration, formal analysis.

## Acknowledgments

We are grateful to William Brock for insightful discussions and for jointly developing the disturbance-risk motivation used in this study. Any remaining errors are our own. The authors gratefully acknowledge the financial contribution of the Project PRIN22 "Impact of the Human Activities on the Environment and Economic Decision Making in a Heterogeneous Setting: Mathematical Models and Policy Implications," Code 20223PNJBK-002- Settore SH7. Generative AI and AI-assisted technologies were used solely to improve language and readability. The authors reviewed the final manuscript and take full responsibility for its content. Open access publishing facilitated by Universita degli Studi di Bologna, as part of the Wiley - CRUI-CARE agreement.

## Conflicts of Interest

The authors declare no conflicts of interest.



19397445, 2026, 3, Downloaded from https://onlinelibrary.wiley.com/doi/10.1111/nrm.70037 by CochraneItalia, Wiley Online Library on [04/07/2026]. See the Terms and Conditions (https://onlinelibrary.wiley.com/terms-and-conditions) on Wiley Online Library for rules of use; OA articles are governed by the applicable Creative Commons License

## Data Availability Statement

Data sharing not applicable to this article as no datasets were generated or analyzed during the current study. The article describes entirely theoretical research.

## Endnotes

[1]IPBES: Intergovernmental Science-Policy Platform on Biodiversity and Ecosystem Services.

[2]This Hamiltonian is written in the normalized normal form of the PMP, with the nonnegative objective multiplier set to one. The abnormal case, in which this multiplier is zero, is not considered because the private-profit component would then vanish from the Hamiltonian, leaving the maximum condition independent of the finite-horizon economic objective. The same convention applies to the cooperative current-value Hamiltonian introduced later (Dorfman 1969; Seierstad and Sydsæter 1987; Hartl et al. 1995).

## References


Agliardi, E., R. Agliardi, and W. Spanjers. 2024. "The Economic Value of Biodiversity Preservation." *Environmental and Resource Economics* 87, no. 6: 1593–1610. https://doi.org/10.1007/s10640-024-00855-0.

Allen, C. R., J. J. Fontaine, K. L. Pope, and A. S. Garmestani. 2011. "Adaptive Management for a Turbulent Future." *Journal of Environmental Management* 92, no. 5: 1339–1345. https://doi.org/10.1016/j.jenvman.2010.11.019.

Allen, L. J. S. 2010. *An Introduction to Stochastic Processes With Applications to Biology* (2nd ed.). CRC Press.

Arjomandi A, P., S. Seyedi, E. Nabavi, and S. Alikhani. 2022. "Exploring Water Governing System Fit Through a Statistical Mechanics Approach." *Water Research* 215: 118272. https://doi.org/10.1016/j.watres.2022.118272.

Arjomandi A, P., S. Seyedi, N. Komendantova, and E. Vahdani Hulasu. 2024. "Vertical Fit of Water Governing Systems: A Regional Assessment." *Current Research in Environmental Sustainability* 7: 100248. https://doi.org/10.1016/j.crsust.2024.100248.

Arjomandi A, P., S. Seyedi, N. Komendantova, M. Yazdanpanah, and M. Mannocchi. 2025. "The Institutional Analysis and Development Framework: A Mathematical Representation in Water Arena." *Current Research in Environmental Sustainability* 10: 100307. https://doi.org/10.1016/j.crsust.2025.100307.

Barbier, E. B. 2011. *Capitalizing on Nature: Ecosystems as Natural Assets*. Cambridge University Press.

Başar, T., and G. J. Olsder. 1999. Dynamic Noncooperative Game Theory (2nd ed.). Society for Industrial and Applied Mathematics.

Baumgärtner, S., and M. F. Quaas. 2010. "Managing Increasing Environmental Risks Through Agrobiodiversity and Agrienvironmental Policies." *Agricultural Economics* 41, no. 5: 483–496. https://doi.org/10.1111/j.1574-0862.2010.00460.x.

Baumgärtner, S., C. Becker, M. Faber, and R. Manstetten. 2006. "Relative and Absolute Scarcity of Nature: Assessing the Roles of Economics and Ecology for Biodiversity Conservation." *Ecological Economics* 59, no. 4: 487–498. https://doi.org/10.1016/j.ecolecon.2005.11.012.

Bongaarts, J. 2019. "IPBES, 2019: Summary for Policymakers of the Global Assessment Report on Biodiversity and Ecosystem Services of the Intergovernmental Science-Policy Platform on Biodiversity and Ecosystem Services." *Population and Development Review* 45, no. 3: 680–681. https://doi.org/10.1111/padr.12283.

Brock, W. A., and A. Xepapadeas. 2002. "Biodiversity Management Under Uncertainty: Species Selection and Harvesting Rules." In *Economic Theory for the Environment: Essays in Honour of Karl-Göran Mäler*, edited by B. Kriström, P. Dasgupta, and K.-G. Löfgren, 62–97. Edward Elgar.

Brock, W. A., and A. Xepapadeas. 2003. "Valuing Biodiversity From an Economic Perspective: A Unified Economic, Ecological, and Genetic Approach." *American Economic Review* 93, no. 5: 1597–1614. https://doi.org/10.1257/000282803322655464.

Brockerhoff, E. G., L. Barbaro, B. Castagneyrol, et al. 2017. "Forest Biodiversity, Ecosystem Functioning and the Provision of Ecosystem Services." *Biodiversity and Conservation* 26, no. 13: 3005–3035. https://doi.org/10.1007/s10531-017-1453-2.

Bryson, A. E. 2018. *Applied Optimal Control: Optimization, Estimation and Control*. Routledge.

Buongiorno, J. 2001. "Generalization of Faustmann's Formula for Stochastic Forest Growth and Prices With Markov Decision Process Models." *Forest Science* 47, no. 4: 466–474. https://doi.org/10.1093/forestscience/47.4.466.

Bush, A., R. Sollmann, A. Wilting, et al. 2017. "Connecting Earth Observation to High-Throughput Biodiversity Data." *Nature Ecology & Evolution* 1: 0176. https://doi.org/10.1038/s41559-017-0176.

Cao, T., K. Hyytiäinen, O. Tahvonen, and L. Valsta. 2006. "Effects of Initial Stand States on Optimal Thinning Regime and Rotation of Picea Abies Stands." *Scandinavian Journal of Forest Research* 21, no. 5: 388–398. https://doi.org/10.1080/02827580600951915.

Cardinale, B. J., J. E. Duffy, A. Gonzalez, et al. 2012. "Biodiversity Loss and Its Impact on Humanity." *Nature* 486, no. 7401: 59–67. https://doi.org/10.1038/nature11148.

Caswell, H. 1989. *Matrix Population Models: Construction, Analysis, and Interpretation*. Sinauer Associates.

Chadès, I., and B. Bouteiller. 2005. "Solving Multiagent Markov Decision Processes: A Forest Management Example." *International Congress on Modelling and Simulation 2005: Advances and Applications for Management and Decision Making* 16: 1594–1600.

Clark, C. W. 2010. *Mathematical Bioeconomics: The Mathematics of Conservation* (3rd ed.). John Wiley & Sons.

Clarke, H. R., and W. J. Reed. 1989. "The Tree-Cutting Problem in a Stochastic Environment." *Journal of Economic Dynamics and Control* 13, no. 4: 569–595. https://doi.org/10.1016/0165-1889(89)90004-3.

Corriga, G., D. Salimbeni, S. Sanna, and G. Usai. 1988. "An Optimal Control Problem in Forest Management." *Applied Mathematical Modelling* 12, no. 3: 328–332. https://doi.org/10.1016/0307-904X(88)90041-8.

Costanza, R., R. de Groot, P. Sutton, et al. 2014. "Changes in the Global Value of Ecosystem Services." *Global Environmental Change* 26: 152–158. https://doi.org/10.1016/j.gloenvcha.2014.04.002.

Dasgupta, P. 2021. "The Economics of Biodiversity: The Dasgupta Review." *HM Treasury* : 610.

Dorfman, R. 1969. "An Economic Interpretation of Optimal Control Theory." *American Economic Review* 59, no. 5: 817–831.

Farley, J., and R. Costanza. 2010. "Payments for Ecosystem Services: From Local to Global." *Ecological Economics* 69, no. 11: 2060–2068. https://doi.org/10.1016/j.ecolecon.2010.06.010.

Faustmann, M. 1849. "Berechnung des Werthes, welchen Waldboden, sowie noch nicht haubare Holzbestände für die Waldwirtschaft besitzen." *Allgemeine Forst- und Jagd-Zeitung* 15: 441–455.

Franklin, J. F., D. Lindenmayer, J. A. MacMahon, et al. 2000. "Threads of Continuity." *Conservation in Practice* 1, no. 1: 8–17. https://doi.org/10.1111/j.1526-4629.2000.tb00155.x.

Grimm, V., E. Revilla, U. Berger, et al. 2005. "Pattern-Oriented Modeling of Agent-Based Complex Systems: Lessons From Ecology." *Science* 310, no. 5750: 987–991. https://doi.org/10.1126/science.1116681.

Haight, R. G., and R. A. Monserud. 1990. "Optimizing Any-Aged Management of Mixed-Species Stands: II. Effects of Decision Criteria."




19397445, 2026, 3, Downloaded from https://onlinelibrary.wiley.com/doi/10.1111/nrm.70037 by CochraneItalia, Wiley Online Library on [04/07/2026]. See the Terms and Conditions (https://onlinelibrary.wiley.com/terms-and-conditions) on Wiley Online Library for rules of use; OA articles are governed by the applicable Creative Commons License

*Forest Science* 36, no. 1: 125–144. https://doi.org/10.1093/forestscience/36.1.125.

Hairer, E., and G. Wanner. 1996. *Solving Ordinary Differential Equations II: Stiff and Differential-Algebraic Problems* (2nd ed.). Springer.

Hairer, E., S. P. Nørsett, and G. Wanner. 1993. *Solving Ordinary Differential Equations I: Nonstiff Problems* (2nd ed.). Springer.

Hale, J. K., and H. Koçak. 1991. *Dynamics and Bifurcations*. Springer.

Hartl, R. F., S. P. Sethi, and R. G. Vickson. 1995. "A Survey of the Maximum Principles for Optimal Control Problems With State Constraints." *SIAM Review* 37, no. 2: 181–218. https://doi.org/10.1137/1037043.

Hong, P., B. Schmid, F. De Laender, et al. 2022. "Biodiversity Promotes Ecosystem Functioning Despite Environmental Change." *Ecology Letters* 25, no. 2: 555–569. https://doi.org/10.1111/ele.13936.

Hyytiäinen, K., and O. Tahvonen. 2003. "Maximum Sustained Yield, Forest Rent or Faustmann: Does It Really Matter?" *Scandinavian Journal of Forest Research* 18, no. 5: 457–469. https://doi.org/10.1080/02827580310013235.

IPBES. 2019. Summary for Policymakers of the Global Assessment Report on Biodiversity and Ecosystem Services of the Intergovernmental Science-Policy Platform on Biodiversity and Ecosystem Services. IPBES Secretariat. https://doi.org/10.5281/zenodo.3553458.

Johnstone, J. F., C. D. Allen, J. F. Franklin, et al. 2016. "Changing Disturbance Regimes, Ecological Memory, and Forest Resilience." *Frontiers in Ecology and the Environment* 14, no. 7: 369–378. https://doi.org/10.1002/fee.1311.

Khalil, H. K. 2002. *Nonlinear Systems* (3rd ed.). Prentice Hall.

Koskela, E., and M. Ollikainen. 2001. "Optimal Private and Public Harvesting Under Spatial and Temporal Interdependence." *Forest Science* 47, no. 4: 484–496. https://doi.org/10.1093/forestscience/47.4.484.

Kushner, H. J. 1990. "Numerical Methods for Stochastic Control Problems in Continuous Time." *SIAM Journal on Control and Optimization* 28, no. 5: 999–1048. https://doi.org/10.1137/0328056.

Lande, R. 1993. "Risks of Population Extinction From Demographic and Environmental Stochasticity and Random Catastrophes." *American Naturalist* 142, no. 6: 911–927. https://doi.org/10.1086/285580.

Lee, J., and W. M. Haddad. 2021. "On Finite-Time Stability and Stabilization of Nonlinear Hybrid Dynamical Systems." *AIMS Mathematics* 6, no. 6: 5535–5562. https://doi.org/10.3934/math.2021328.

Lembersky, M. R. 1978. "The Application of Markov Decision Processes to Forest Management." In *Dynamic Programming and Its Applications*, edited by R. E. Bellman and S. E. Dreyfus, 207–219. Academic Press.

Loisel, P. 2014. "Impact of Storm Risk on Faustmann Rotation." *Forest Policy and Economics* 38: 191–198. https://doi.org/10.1016/j.forpol.2013.08.002.

Loreau, M., and A. Hector. 2001. "Partitioning Selection and Complementarity in Biodiversity Experiments." *Nature* 412, no. 6842: 72–76. https://doi.org/10.1038/35083573.

Montgomery, C. A., and D. M. Adams. 1995. "Optimal Timber Management Policies." In *The Handbook of Environmental Economics*, edited by D. W. Bromley, 379–404. Blackwell.

Naeem, S., Bunker, D. E., Hector, A., Loreau, M., and Perrings, C., ed. 2009. *Biodiversity, Ecosystem Functioning, and Human Wellbeing: An Ecological and Economic Perspective*. Oxford University Press.

Nagumo, M. 1942. "Über die Lage der Integralkurven gewöhnlicher Differentialgleichungen." *Proceedings of the Physico-Mathematical Society of Japan, 3rd Series* 24: 551–559.

Øksendal, B., and A. Sulem. 2007. *Applied Stochastic Control of Jump Diffusions* (2nd ed.). Springer.

Oliveira, B. F., F. C. Moore, and X. Dong. 2022. "Biodiversity Mediates Ecosystem Sensitivity to Climate Variability." *Communications Biology* 5: 628. https://doi.org/10.1038/s42003-022-03573-9.

Ostrom, E. 2009. "A General Framework for Analyzing Sustainability of Social-Ecological Systems." *Science* 325, no. 5939: 419–422. https://doi.org/10.1126/science.1172133.

Puettmann, K. J., K. D. Coates, and C. C. Messier. 2012. *A Critique of Silviculture: Managing for Complexity*. Island Press.

Reed, W. J. 1979. "Optimal Escapement Levels in Stochastic and Deterministic Harvesting Models." *Journal of Environmental Economics and Management* 6, no. 4: 350–363. https://doi.org/10.1016/0095-0696(79)90014-7.

Reed, W. J. 1984. "The Effects of the Risk of Fire on the Optimal Rotation of a Forest." *Journal of Environmental Economics and Management* 11, no. 2: 180–190. https://doi.org/10.1016/0095-0696(84)90016-0.

Reed, W. J. 1988. "Optimal Harvesting of a Fishery Subject to Random Catastrophic Collapse." *Mathematical Medicine and Biology* 5, no. 3: 215–235. https://doi.org/10.1093/imammb/5.3.215.

Reuters. 2024. *World Bank Prices $225 Million Bond Linked to Amazon Reforestation*. Reuters.

Rockström, J., W. Steffen, K. Noone, et al. 2009. "A Safe Operating Space for Humanity." *Nature* 461, no. 7263: 472–475. https://doi.org/10.1038/461472a.

Routledge, R. D. 1980. "The Effect of Potential Catastrophic Mortality and Other Unpredictable Events on Optimal Forest Rotation Policy." *Forest Science* 26, no. 3: 389–399. https://doi.org/10.1093/forestscience/26.3.389.

Scheffer, M., S. Carpenter, J. A. Foley, C. Folke, and B. Walker. 2001. "Catastrophic Shifts in Ecosystems." *Nature* 413, no. 6856: 591–596. https://doi.org/10.1038/35098000.

Schreuder, G. F. 1971. "The Simultaneous Determination of Optimal Thinning Schedule and Rotation for an Even-Aged Forest." *Forest Science* 17, no. 3: 333–339. https://doi.org/10.1093/forestscience/17.3.333.

Seierstad, A., and K. Sydsæter. 1987. *Optimal Control Theory With Economic Applications*. North-Holland.

Seyedi, S. 2010. Cutting Angle Method for Optimal Control Problems [Master's Thesis, Universiti Teknologi Malaysia].

Seyedi, S., I. S. Amiri, S. Chaghervand, and V. J. Sorger. 2018. *The Numerical Solution of Continuous Time Optimal Control Problems With the Cutting Angle Method*. Nova Science Publishers.

Snyder, D. L., and R. N. Bhattacharyya. 1990. "A More General Dynamic Economic Model of the Optimal Rotation of Multiple-Use Forests." *Journal of Environmental Economics and Management* 18, no. 2: 168–175. https://doi.org/10.1016/0095-0696(90)90046-2.

Spittlehouse, D. L., and R. B. Stewart. 2004. "Adaptation to Climate Change in Forest Management." *Journal of Ecosystems and Management* 4, no. 1: 1–11. https://doi.org/10.22230/jem.2004v4n1a254.

Stoer, J., and R. Bulirsch. 2002. *Introduction to Numerical Analysis* (3rd ed.). Springer.

Swallow, S. K., and D. N. Wear. 1993. "Spatial Interactions in Multiple-Use Forestry and Substitution and Wealth Effects for the Single Stand." *Journal of Environmental Economics and Management* 25, no. 2: 103–120. https://doi.org/10.1006/jeem.1993.1036.

Teschl, G. 2012. *Ordinary Differential Equations and Dynamical Systems*. American Mathematical Society.

Thorsen, B. J., and F. Helles. 1998. "Optimal Stand Management With Endogenous Risk of Sudden Destruction." *Forest Ecology and Management* 108, no. 3: 287–299. https://doi.org/10.1016/S0378-1127(97)00300-3.



19397445, 2026, 3, Downloaded from https://onlinelibrary.wiley.com/doi/10.1111/nrm.70037 by CochraneItalia, Wiley Online Library on [04/07/2026]. See the Terms and Conditions (https://onlinelibrary.wiley.com/terms-and-conditions) on Wiley Online Library for rules of use; OA articles are governed by the applicable Creative Commons License

Tilman, D., D. Wedin, and J. Knops. 1996. "Productivity and Sustainability Influenced by Biodiversity in Grassland Ecosystems." *Nature* 379, no. 6567: 718–720. https://doi.org/10.1038/379718a0.

Tilman, D., P. B. Reich, and J. M. H. Knops. 2006. "Biodiversity and Ecosystem Stability in a Decade-Long Grassland Experiment." *Nature* 441, no. 7093: 629–632. https://doi.org/10.1038/nature04742.

Touza, J., M. Termansen, and C. Perrings. 2008. "A Bioeconomic Approach to the Faustmann-Hartman Model: Ecological Interactions in Managed Forest." *Natural Resource Modeling* 21, no. 4: 551–581. https://doi.org/10.1111/j.1939-7445.2008.00023.x.

Turner, M. G. 2010. "Disturbance and Landscape Dynamics in a Changing World." *Ecology* 91, no. 10: 2833–2849. https://doi.org/10.1890/10-0097.1.

Vardas, G., and A. Xepapadeas. 2010. "Model Uncertainty, Ambiguity and the Precautionary Principle: Implications for Biodiversity Management." *Environmental and Resource Economics* 45, no. 3: 379–404. https://doi.org/10.1007/s10640-009-9318-z.

Walters, C. J., and C. S. Holling. 1990. "Large-Scale Management Experiments and Learning by Doing." *Ecology* 71, no. 6: 2060–2068. https://doi.org/10.2307/1938620.

Willassen, Y. 1998. "The Stochastic Rotation Problem: A Generalization of Faustmann's Formula to Stochastic Forest Growth." *Journal of Economic Dynamics and Control* 22, no. 4: 573–596. https://doi.org/10.1016/S0165-1889(97)00071-7.

Wunder, S. 2005. Payments for Environmental Services: Some Nuts and Bolts (CIFOR Occasional Paper No. 42). Center for International Forestry Research.

Wunder, S. 2015. "Revisiting the Concept of Payments for Environmental Services." *Ecological Economics* 117: 234–243. https://doi.org/10.1016/j.ecolecon.2014.08.016.

Xepapadeas, A. 2022. "On the Optimal Management of Environmental Stock Externalities." *Proceedings of the National Academy of Sciences* 119, no. 24: e2202679119. https://doi.org/10.1073/pnas.2202679119.

## Supporting Information

Additional supporting information can be found online in the Supporting Information section.
**Supporting File:** nrm70037-sup-0001-Supplementary_Material_R2_clean.docx.

## Appendix A
## Steady states and local properties of the deterministic ecological subsystem

This appendix records the steady states and local linearization of the deterministic ecological subsystem used in the main text. The disturbance component enters only through the expected-drift term $\varpi\kappa$. Thus, the analysis below concerns the deterministic benchmark, not stochastic sample paths.

Let

$$U(t) = \sum_{i=1}^{n} u_i(t) \tag{A.1}$$

denote aggregate harvest. The ecological subsystem is

$$\begin{aligned} \dot{x}(t) &= r(B(t))x(t)\left(1 - \frac{x(t)}{K}\right) - U(t), r(B(t)) \\ &= AB(t)^{\zeta}, 0 < \zeta \le 1, \end{aligned} \tag{A.2}$$

$$\dot{B}(t) = gB(t) - \delta Z(t) - \varpi\kappa, \dot{Z}(t) = U(t) - \gamma Z(t), \tag{A.3}$$

with $A, K, g, \delta, \gamma > 0$. For closed-form characterization, set $U(t) = \bar{U}$. A steady state $(x^*, B^*, Z^*)$ satisfies

$$Z^* = \frac{\bar{U}}{\gamma}, B^* = \frac{\delta\bar{U}/\gamma + \varpi\kappa}{g}. \tag{A.4}$$

Let

$$r^* = r(B^*) = A(B^*)^{\zeta}. \tag{A.5}$$

The biomass steady state is determined by

$$r^*x^*\left(1 - \frac{x^*}{K}\right) = \bar{U}. \tag{A.6}$$

Equivalently,

$$\frac{r^*}{K}(x^*)^2 - r^*x^* + \bar{U} = 0, \tag{A.7}$$

so real biomass steady states exist if and only if

$$0 \le \bar{U} \le \frac{r^*K}{4}. \tag{A.8}$$

When Equation (A.8) holds,

$$x^*_{\pm} = \frac{K}{2}\left[1 \pm \sqrt{1 - \frac{4\bar{U}}{r^*K}}\right]. \tag{A.9}$$

The branch $x^*_+ > \frac{K}{2}$ is the high-biomass branch, and $x^*_- < \frac{K}{2}$ is the low-biomass branch. At $\bar{U} = \frac{r^*K}{4}$, the two branches coincide at $x^* = \frac{K}{2}$.

The Jacobian of Equations (A.2–A.3) at $(x^*, B^*, Z^*)$ is

$$J^* = \begin{pmatrix} r^*\left(1 - \frac{2x^*}{K}\right) & r'(B^*)x^*\left(1 - \frac{x^*}{K}\right) & 0 \\ 0 & g & -\delta \\ 0 & 0 & -\gamma \end{pmatrix}, \tag{A.10}$$

$$r'(B) = A\zeta B^{\zeta-1}.$$

Since $J^*$ is upper triangular,

$$\eta_1 = r^*\left(1 - \frac{2x^*}{K}\right), \quad \eta_2 = g, \quad \eta_3 = -\gamma. \tag{A.11}$$

Hence the cumulative-pressure direction is locally stable because $\eta_3 < 0$. The biomass direction is locally stable on the high-biomass branch and locally unstable on the low-biomass branch:

$$x^*_+ > \frac{K}{2} \Rightarrow \eta_1 < 0, \quad x^*_- < \frac{K}{2} \Rightarrow \eta_1 > 0. \tag{A.12}$$

The benchmark linear biodiversity equation has $\eta_2 = g$. Since the calibration treats $g > 0$ as a regenerative-capacity parameter, this linear constant-harvest subsystem is locally repelling in the biodiversity direction. Accordingly, Equation (A.3) is used as a finite-horizon benchmark rather than as a globally stabilizing ecological law. Appendix B therefore examines nonlinear regeneration–damage specifications that introduce concavity in biodiversity recovery and nonlinear cumulative-pressure effects.



19397445, 2026, 3, Downloaded from https://onlinelibrary.wiley.com/doi/10.1111/nrm.70037 by CochraneItalia, Wiley Online Library on [04/07/2026]. See the Terms and Conditions (https://onlinelibrary.wiley.com/terms-and-conditions) on Wiley Online Library for rules of use; OA articles are governed by the applicable Creative Commons License

These local results apply only to the constant-harvest ecological subsystem. In the full model, harvest is endogenous and determined by the finite-horizon Pontryagin system. Under symmetry and quadratic harvesting costs,

$$u_i^*(t) = u^*(t) = \max\left\{0, \frac{p(t) - \lambda(t) + \nu(t)}{\alpha_C}\right\}, U^*(t) = nu^*(t). \quad \text{(A.13)}$$

Thus, the simulated paths are governed by the forward–backward boundary-value problem, with initial states, endpoint restrictions, and transversality conditions jointly determining the finite-horizon trajectory. This appendix provides local analytical context for the deterministic simulations; it does not establish global stability or stochastic sample-path properties.

## Appendix B
## Nonlinear biodiversity dynamics and robustness

This appendix examines whether the regime comparisons depend on the benchmark linear biodiversity law. Replace

$$G(B(t), Z(t)) = gB(t) - \delta Z(t), \quad \text{(B.1)}$$

with

$$G(B(t), Z(t)) = gB(t)^a - \delta Z(t)^b, \quad 0 < a \le 1, \quad b \ge 1, \quad \text{(B.2)}$$

so that

$$\dot{B}(t) = gB(t)^a - \delta Z(t)^b - \varpi\kappa. \quad \text{(B.3)}$$

Here $g, \delta > 0$ and $\varpi\kappa$ is the expected disturbance-loss term defined in the main text. On the interior domain $B(t) > 0, Z(t) > 0$,

$$\begin{aligned} G_B &= \frac{\partial G}{\partial B} = gaB(t)^{a-1} > 0, \\ G_{BB} &= \frac{\partial^2 G}{\partial B^2} = ga(a-1)B(t)^{a-2} \le 0, \end{aligned} \quad \text{(B.4)}$$

and

$$\begin{aligned} G_Z &= \frac{\partial G}{\partial Z} = -\delta bZ(t)^{b-1} < 0, \\ G_{ZZ} &= \frac{\partial^2 G}{\partial Z^2} = -\delta b(b-1)Z(t)^{b-2} \le 0, \end{aligned} \quad \text{(B.5)}$$

Thus, biodiversity regeneration is positive and weakly concave in $B(t)$, while cumulative harvesting pressure reduces biodiversity growth. When $b > 1$, the marginal damage of cumulative harvesting pressure becomes increasingly negative as $Z(t)$ rises. The baseline linear case is recovered when $a = b = 1$.

The state equations become

$$\dot{x}(t) = r(B(t))x(t)\left(1 - \frac{x(t)}{K}\right) - U(t), \quad \text{(B.6)}$$

$$\dot{B}(t) = gB(t)^a - \delta Z(t)^b - \varpi\kappa, \quad \text{(B.7)}$$

$$\dot{Z}(t) = U(t) - \gamma Z(t). \quad \text{(B.8)}$$

The Pontryagin structure is unchanged; only the costate equations involving $G_B$ and $G_Z$ are modified. In the cooperative case, the biodiversity and cumulative-harvesting-pressure costate become

$$\begin{aligned} \dot{\mu}(t) = \rho\mu(t) - \Big[V_1'(B(t)) + \lambda(t)r'(B(t))x(t)\Big(1 - \frac{x(t)}{K}\Big) \\ + gaB(t)^{a-1}\mu(t)\Big], \end{aligned} \quad \text{(B.9)}$$

$$\begin{aligned} \dot{\nu}(t) = \rho\nu(t) - [-\delta bZ(t)^{b-1}\mu(t) - \gamma\nu(t)] = (\rho + \gamma)\nu \\ (t) + \delta bZ(t)^{b-1}\mu(t). \end{aligned} \quad \text{(B.10)}$$

The first-order harvesting condition is unchanged in form because controls enter through biomass extraction and cumulative harvesting pressure. Under symmetry and quadratic harvesting costs,

$$u_i^*(t) = u^*(t) = \max\left\{0, \frac{p(t) - \lambda(t) + \nu(t)}{\alpha_C}\right\}. \quad \text{(B.11)}$$

To compare curvature variants without changing the initial magnitude of regeneration or damage, parameters are normalized at $(B_0, Z_0)$. Let $g_1$ and $\delta_1$ denote the linear benchmark parameters. Define

$$g(a) = g_1 B_0^{1-a}, \quad \delta(b) = \delta_1 Z_0^{1-b}. \quad \text{(B.12)}$$

Then

$$g(a)B_0^a = g_1 B_0, \quad \delta(b)Z_0^b = \delta_1 Z_0. \quad \text{(B.13)}$$

Hence the linear and nonlinear specifications coincide at the initial state, and differences in trajectories arise from curvature rather than from different initial regeneration or damage levels.

Robustness checks are conducted over representative curvature values such as

$$a \in \{0.6, 0.8, 1\}, \quad b \in \{1, 1.5, 2\}. \quad \text{(B.14)}$$

Within the calibrated deterministic benchmark, the qualitative regime ranking remains consistent with the main results. Cooperative governance continues to generate more favorable ecological and objective-value outcomes than the noncooperative benchmark, while the free-endpoint cooperative design remains less constrained by terminal state requirements. These results should be interpreted as local robustness evidence around the calibrated parameterization, consistent with the sensitivity protocol in Supporting Information S1 and the baseline calibration in Supporting Information S2, rather than as global robustness over the full parameter space.

## Appendix C
## (Non) Cooperative Solution's Wolfram Mathematica 14.2 Code

```
(*=========================================
==========================*)(*F

INITE-HORIZON PONTRYAGIN SYSTEMS (Choice 1,u>=0 enforced)
*)(*-OLNE:\

Fixed/Free endpoints*)(*-Regulator:Fixed/\
```



19397445, 2026, 3, Downloaded from https://onlinelibrary.wiley.com/doi/10.1111/nrm.70037 by CochraneItalia, Wiley Online Library on [04/07/2026]. See the Terms and Conditions (https://onlinelibrary.wiley.com/terms-and-conditions) on Wiley Online Library for rules of use; OA articles are governed by the applicable Creative Commons License

```
Free endpoints*)(*Choice 1 consistency:V1(B)=n*Sqrt[B],V2(x)=n*Log[x]*)(*================================================================*)

ClearAll["Global`*"];

(*-------------------------------------------------------------*)

(*0) Time horizon*)

(*-------------------------------------------------------------*)

t0 = 0; (*initial time*)

tf = 20; (*terminal time*)

(*-------------------------------------------------------------*)

(*1) System parameters*)

(*-------------------------------------------------------------*)

n = 15;

K = 1000;

delta = 0.1;

g = 0.2;

gamma = 0.3;

jump = 0.0001; (*jump=varpi*k (expected-drift loss term)*)

(*Biomass growth r(B)=A B^xi*)

A = 0.00002;

xi = 1; (*0<xi<=1*)

r[B_] := A B^xi;

rprime[B_] := A xi B^(xi - 1);

(*Objective parameters*)

rho = 0.01;

piVal = 40; (*constant biomass price*)

alphaC = 100; (*quadratic cost coefficient*)

p[s_?NumericQ] := piVal;

c[u_?NumericQ] := (alphaC/2) u^2;

(*-------------------------------------------------------------*)

(*2) Enforcing u(t)>=0:projection (exact) or smooth (robust)*)

(*-------------------------------------------------------------*)

useSmooth =

True; \

(*recommended for BVP convergence; set False for exact Max[]*)

kappa = 50; \

(*smoothing sharpness; larger-> closer to Max[0,z]*)

uSmooth[z_] := (1/kappa) Log[

1 + Exp[kappa z]]; (*softplus approximation*)

uProj[z_] := Max[0, z];

uFromCostates[lam_, vv_] := Module[{z}, z = (piVal - lam + vv)/alphaC;

If[useSmooth, uSmooth[z], uProj[z]]];

(*-------------------------------------------------------------*)

(*3) Boundary conditions*)

(*-------------------------------------------------------------*)

x0 = 500; B0 = 10; Z0 = 0.1;

xF = 400; BF = 150; ZF = 10;

(*================================================================*)

(*1) OLNE Solution:Fixed Terminal BCs*)

(*================================================================*)

solOLNEFixed =

NDSolve[{(*State equations*)

x'[t] ==

r[B[t]] x[t] (1 - x[t]/K) - n*uFromCostates[\[Lambda][t], v[t]],

B'[t] == g B[t] - delta Z[t] - jump,

Z'[t] ==

n*uFromCostates[\[Lambda][t], v[t]] -

gamma Z[t],(*Costate equations (current value)*)\[Lambda]'[t] ==

rho \[Lambda][t] - \[Lambda][t] r[B[t]] (1 - 2 x[t]/K), \[Mu]'[

t] == rho \[Mu][t] - \[Lambda][t] rprime[B[t]] x[

t] (1 - x[t]/K) - g \[Mu][t],

v'[t] == (rho + gamma) v[t] +

delta \[Mu][t],(*Fixed terminal BCs on states*)x[0] == x0,

B[0] == B0, Z[0] == Z0, x[tf] == xF, B[tf] == BF,

Z[tf] == ZF}, {x, B, Z, \[Lambda], \[Mu], v}, {t, t0, tf},

Method -> "StiffnessSwitching", WorkingPrecision -> 30];
```



19397445, 2026, 3, Downloaded from https://onlinelibrary.wiley.com/doi/10.1111/nrm.70037 by CochraneItalia, Wiley Online Library on [04/07/2026]. See the Terms and Conditions (https://onlinelibrary.wiley.com/terms-and-conditions) on Wiley Online Library for rules of use; OA articles are governed by the applicable Creative Commons License

```
(*Extract solution functions*)

xOLNEFixed[t_] := x[t] /. solOLNEFixed[[1]];

BOLNEFixed[t_] := B[t] /. solOLNEFixed[[1]];

ZOLNEFixed[t_] := Z[t] /. solOLNEFixed[[1]];

\[Lambda]OLNEFixed[t_] := \[Lambda][t] /. solOLNEFixed[[1]];

\[Mu]OLNEFixed[t_] := \[Mu][t] /. solOLNEFixed[[1]];

vOLNEFixed[t_] := v[t] /. solOLNEFixed[[1]];

uOLNEFixed[t_] := uFromCostates[\[Lambda]OLNEFixed[t], vOLNEFixed[t]];

(*OLNE (market) objective per agent*)

JOLNEFixed[t_?NumericQ] :=

NIntegrate[

Exp[-rho s] (p[s] uOLNEFixed[s] - c[uOLNEFixed[s]]), {s, t0, t},

Method -> {"LocalAdaptive"}];

JOLNEFixedTotal =

NIntegrate[

Exp[-rho s] (p[s] uOLNEFixed[s] - c[uOLNEFixed[s]]), {s, t0, tf},

Method -> {"LocalAdaptive"}];

Print["(OLNE-Fixed) Discounted profit per agent over [0, ", tf, "] = ",

JOLNEFixedTotal];

(*========================================
======================*)

(*2) OLNE Solution:Free Terminal BCs*)

(*=======================================
=========================*)

solOLNEFree =

NDSolve[{(*State equations*)

x'[t] ==

r[B[t]] x[t] (1 - x[t]/K) - n*uFromCostates[\[Lambda][t], v[t]],

B'[t] == g B[t] - delta Z[t] - jump,

Z'[t] ==

n*uFromCostates[\[Lambda][t], v[t]] -

gamma Z[t],(*Costate equations*)\[Lambda]'[t] ==

rho \[Lambda][t] - \[Lambda][t] r[B[t]] (1 - 2 x[t]/K), \[Mu]'

[t] == rho \[Mu][t] - \[Lambda][t] rprime[B[t]]

x[t] (1 - x[t]/K) - g \[Mu][t],

v'[t] == (rho + gamma) v[t] +

delta \[Mu][t],(*Free terminal BCs on costates*)x[0] == x0,

B[0] == B0, Z[0] == Z0, \[Lambda][tf] == 0, \[Mu][tf] == 0,

v[tf] == 0}, {x, B, Z, \[Lambda], \[Mu], v}, {t, t0, tf},

Method -> "StiffnessSwitching", WorkingPrecision -> 30];

(*Extract solution functions*)

xOLNEFree[t_] := x[t] /. solOLNEFree[[1]];

BOLNEFree[t_] := B[t] /. solOLNEFree[[1]];

ZOLNEFree[t_] := Z[t] /. solOLNEFree[[1]];

\[Lambda]OLNEFree[t_] := \[Lambda][t] /. solOLNEFree[[1]];

\[Mu]OLNEFree[t_] := \[Mu][t] /. solOLNEFree[[1]];

vOLNEFree[t_] := v[t] /. solOLNEFree[[1]];

uOLNEFree[t_] := uFromCostates[\[Lambda]OLNEFree[t], vOLNEFree[t]];

(*OLNE (market) objective per agent*)

JOLNEFree[t_?NumericQ] :=

NIntegrate[

Exp[-rho s] (p[s] uOLNEFree[s] - c[uOLNEFree[s]]), {s, t0, t},

Method -> {"LocalAdaptive"}];

JOLNEFreeTotal =

NIntegrate[

Exp[-rho s] (p[s] uOLNEFree[s] - c[uOLNEFree[s]]), {s, t0, tf},

Method -> {"LocalAdaptive"}];

Print["(OLNE-Free) Discounted profit per agent over [0, ", tf, "] = ",

JOLNEFreeTotal];

(*=====================================
============================*)

(*3) Regulator Solution:Fixed Terminal BCs (Choice 1 scaling)*)

(*==============================
================================*)

(*Consistency note (Choice 1):Non-market values are V1(B)=n*Sqrt[B],

V2(x)=n*Log[x].Hence V1'(B)=n/(2*Sqrt[B]) and V2'(x)=n/x,
```



19397445, 2026, 3, Downloaded from https://onlinelibrary.wiley.com/doi/10.1111/nrm.70037 by CochraneItalia, Wiley Online Library on [04/07/2026]. See the Terms and Conditions (https://onlinelibrary.wiley.com/terms-and-conditions) on Wiley Online Library for rules of use; OA articles are governed by the applicable Creative Commons License

```
which appear below.*)
solRegFixed =
NDSolve[{(*State equations*)
x'[t] ==
r[B[t]] x[t] (1 - x[t]/K) - n*uFromCostates[\[Lambda][t], v[t]],
B'[t] == g B[t] - delta Z[t] - jump,
Z'[t] ==
n*uFromCostates[\[Lambda][t], v[t]] -
gamma Z[t],(*Planner costate equations (current value)*)\
\[Lambda]'[t] ==
rho \[Lambda][
t] - ((n/x[t]) + \[Lambda][t] r[B[t]] (1 - 2 x[t]/K)), \[Mu]'[
t] == rho \[Mu][
t] - ((n/(2 Sqrt[B[t]])) + \[Lambda][t] rprime[B[t]] x[
t] (1 - x[t]/K) + g \[Mu][t]),
v'[t] == (rho + gamma) v[t] +
delta \[Mu][t],(*Fixed terminal BCs on states*)x[0] == x0,
B[0] == B0, Z[0] == Z0, x[tf] == xF, B[tf] == BF,
Z[tf] == ZF}, {x, B, Z, \[Lambda], \[Mu], v}, {t, t0, tf},
Method -> {"Shooting,"
"ImplicitSolver" -> {"Newton," "StepControl" -> "LineSearch"}},
WorkingPrecision -> 30];
(*Extract solution functions*)
xRegFixed[t_] := x[t] /. solRegFixed[[1]];
BRegFixed[t_] := B[t] /. solRegFixed[[1]];
ZRegFixed[t_] := Z[t] /. solRegFixed[[1]];
\[Lambda]RegFixed[t_] := \[Lambda][t] /. solRegFixed[[1]];
\[Mu]RegFixed[t_] := \[Mu][t] /. solRegFixed[[1]];
vRegFixed[t_] := v[t] /. solRegFixed[[1]];
uRegFixed[t_] := uFromCostates[\[Lambda]RegFixed[t], vRegFixed[t]];
(*Regulator objective integrand (Choice 1:scale ecological terms by n)*)
RegIntegrandFixed[t_?NumericQ] :=
Exp[-rho t]*(n (p[t] uRegFixed[t] - c[uRegFixed[t]]) +
n*Sqrt[BRegFixed[t]] + n*Log[xRegFixed[t]]);
RegObjFixed[t_?NumericQ] :=
NIntegrate[RegIntegrandFixed[s], {s, t0, t}, PrecisionGoal -> 10,
Method -> {"LocalAdaptive"}];
RegObjFixedTotal =
NIntegrate[RegIntegrandFixed[s], {s, t0, tf}, PrecisionGoal -> 10,
Method -> {"LocalAdaptive"}];
Print["(Reg-Fixed) Regulator objective over [0, ", tf, "] = ",
RegObjFixedTotal];
(*=======================================
=======================*)
(*4) Regulator Solution:Free Terminal BCs (Choice 1 scaling)*)
(*=================================
============================*)
solRegFree =
NDSolve[{(*State equations*)
x'[t] ==
r[B[t]] x[t] (1 - x[t]/K) - n*uFromCostates[\[Lambda][t], v[t]],
B'[t] == g B[t] - delta Z[t] - jump,
Z'[t] ==
n*uFromCostates[\[Lambda][t], v[t]] -
gamma Z[t],(*Planner costate equations*)\[Lambda]'[t] ==
rho \[Lambda][
t] - ((n/x[t]) + \[Lambda][t] r[B[t]] (1 - 2 x[t]/K)), \[Mu]'[
t] == rho \[Mu][
t] - ((n/(2 Sqrt[B[t]])) + \[Lambda][t] rprime[B[t]] x[
t] (1 - x[t]/K) + g \[Mu][t]),
v'[t] == (rho + gamma) v[t] +
delta \[Mu][t],(*Free terminal BCs on costates*)x[0] == x0,
B[0] == B0, Z[0] == Z0, \[Lambda][tf] == 0, \[Mu][tf] == 0,
v[tf] == 0}, {x, B, Z, \[Lambda], \[Mu], v}, {t, t0, tf},
Method -> "StiffnessSwitching", WorkingPrecision -> 30];
(*Extract solution functions*)
xRegFree[t_] := x[t] /. solRegFree[[1]];
```



19397445, 2026, 3, Downloaded from https://onlinelibrary.wiley.com/doi/10.1111/nrm.70037 by CochraneItalia, Wiley Online Library on [04/07/2026]. See the Terms and Conditions (https://onlinelibrary.wiley.com/terms-and-conditions) on Wiley Online Library for rules of use; OA articles are governed by the applicable Creative Commons License

```
BRegFree[t_] := B[t] /. solRegFree[[1]];
ZRegFree[t_] := Z[t] /. solRegFree[[1]];
\[Lambda]RegFree[t_] := \[Lambda][t] /. solRegFree[[1]];
\[Mu]RegFree[t_] := \[Mu][t] /. solRegFree[[1]];
vRegFree[t_] := v[t] /. solRegFree[[1]];
uRegFree[t_] := uFromCostates[\[Lambda]RegFree[t], vRegFree[t]];
(*Regulator objective integrand (Choice 1)*)
RegIntegrandFree[t_?NumericQ] :=
Exp[-rho t]*(n (p[t] uRegFree[t] - c[uRegFree[t]]) +
n*Sqrt[BRegFree[t]] + n*Log[xRegFree[t]]);
RegObjFree[t_?NumericQ] :=
NIntegrate[RegIntegrandFree[s], {s, t0, t}, PrecisionGoal -> 10,
Method -> {"LocalAdaptive"}];
RegObjFreeTotal =
NIntegrate[RegIntegrandFree[s], {s, t0, tf}, PrecisionGoal -> 10,
Method -> {"LocalAdaptive"}];
Print["(Reg-Free) Regulator objective over [0, ", tf, "] = ",
RegObjFreeTotal];
(*========================================
========================*)
(*Plot Styles and Comparison Plots*)
(*================================
============================*)
lineStyles3 = {{Darker[Blue], Thick,
Dashing[{0.02, 0.01}]}, {Darker[Red], Thick,
Dashing[{0.06, 0.02}]}, {Darker[Green], Thick,
Dashing[{0.02, 0.02, 0.005, 0.02}]}};
(*1) Biomass x(t)*)
plotX = Plot[{xOLNEFree[t], xRegFixed[t], xRegFree[t]}, {t, t0, tf},
PlotStyle -> lineStyles3, PlotLabel -> "Biomass Comparison,"
PlotLegends -> {"OLNE-Free," "Reg-Fixed," "Reg-Free"},
AxesLabel -> {"t", "x(t)"}];
(*2) Biodiversity B(t)*)
plotB = Plot[{BOLNEFree[t], BRegFixed[t], BRegFree[t]}, {t, t0, tf},
PlotStyle -> lineStyles3, PlotLabel -> "Biodiversity Comparison",
PlotLegends -> {"OLNE-Free," "Reg-Fixed," "Reg-Free"},
AxesLabel -> {"t", "B(t)"}];
(*3) Cumulative harvesting Z(t)*)
plotZ = Plot[{ZOLNEFree[t], ZRegFixed[t], ZRegFree[t]}, {t, t0, tf},
PlotStyle -> lineStyles3,
PlotLabel -> "Cumulative Harvesting Comparison,"
PlotLegends -> {"OLNE-Free," "Reg-Fixed," "Reg-Free"},
AxesLabel -> {"t", "Z(t)"}];
(*4) Costate lambda(t)*)
plotLambda =
Plot[{\[Lambda]OLNEFree[t], \[Lambda]RegFixed[t], \[Lambda]RegFree[
t]}, {t, t0, tf}, PlotStyle -> lineStyles3,
PlotLabel -> "Costate \[Lambda](t) Comparison",
PlotLegends -> {"OLNE-Free", "Reg-Fixed", "Reg-Free"},
AxesLabel -> {"t", "\[Lambda](t)"}];
(*5) Costate mu(t)*)
plotMu =
Plot[{\[Mu]OLNEFree[t], \[Mu]RegFixed[t], \[Mu]RegFree[t]}, {t, t0,
tf}, PlotStyle -> lineStyles3,
PlotLabel -> "Costate \[Mu](t) Comparison",
PlotLegends -> {"OLNE-Free", "Reg-Fixed", "Reg-Free"},
AxesLabel -> {"t", "\[Mu](t)"}];
(*6) Costate v(t)*)
plotv = Plot[{vOLNEFree[t], vRegFixed[t], vRegFree[t]}, {t, t0, tf},
PlotStyle -> lineStyles3, PlotLabel -> "Costate v(t) Comparison",
PlotLegends -> {"OLNE-Free", "Reg-Fixed", "Reg-Free"},
AxesLabel -> {"t", "v(t)"}];
(*7) Control u(t)*)
plotu = Plot[{uOLNEFree[t], uRegFixed[t], uRegFree[t]}, {t, t0, tf},
PlotStyle -> lineStyles3,
PlotLabel -> "Harvest Control u(t) Comparison (u >= 0 enforced)",
PlotLegends -> {"OLNE-Free", "Reg-Fixed", "Reg-Free"},
```



19397445, 2026, 3, Downloaded from https://onlinelibrary.wiley.com/doi/10.1111/nrm.70037 by CochraneItalia, Wiley Online Library on [04/07/2026]. See the Terms and Conditions (https://onlinelibrary.wiley.com/terms-and-conditions) on Wiley Online Library for rules of use; OA articles are governed by the applicable Creative Commons License

```
AxesLabel -> {"t", "u(t)"}];
(*Combined objective plot*)
plotAllObjectives =
Plot[{JOLNEFree[t], RegObjFixed[t], RegObjFree[t]}, {t, t0, tf},
PlotStyle -> lineStyles3,
PlotLabel ->
"Objective Comparison (OLNE per-agent vs. Regulator total)",
PlotLegends -> {"OLNE-Free (per agent)", "Reg-Fixed (total)",
"Reg-Free (total)"}, AxesLabel -> {"t", "Objective Value"}];
(*Display plots*)
Print[plotX];
Print[plotB];
Print[plotZ];
Print[plotLambda];
Print[plotMu];
Print[plotv];
Print[plotu];
Print[plotAllObjectives];
(*========================================
==========================*)
(*Notes:-If convergence is difficult under exact projection u=Max[0,z],\
keep useSmooth=True and raise kappa gradually (e.g., 30-> 50-> 80).\
-For strict projection,set useSmooth=False.*)
(*============================
==================================*)
Sensitive Analysis' Wolfram Mathematica 14.2 Code
(*================================
================================*)(*S
ensitivity Analysis (Finite-horizon Pontryagin BVPs)*)(*-Local (time-\
varying) sensitivities via centered differences*)(*-Parameters:\
{\[Delta],g,\[Rho],\[Gamma],p,jump=\[CurlyPi]    k}*)(*-Regimes:OLN
E-\
Fixed,OLNE-Free,Regulator-Fixed,Regulator-\
Free*)(*-Control constraint u(t)>=0 enforced via smooth projection*)
(*========================================
========================*)
ClearAll["Global`*"];
(*-------------------------------------------------------------*)
(*1) Time span*)
t0 = 0;
tf = 20;
(*-------------------------------------------------------------*)
(*2) Fixed model parameters (NOT in paramVars)*)
n = 15;
K = 1000;
A = 2*10^-5;
\[Xi] = 1;
\[Alpha]C = 100;
r[B_] := A B^\[Xi];
rprime[B_] := A \[Xi] B^(\[Xi] - 1);
(*-------------------------------------------------------------*)
(*3) Boundary data for states*)
{x0, B0, Z0} = {500, 10, 0.1};
{xF, BF, ZF} = {400, 150, 10};
(*-------------------------------------------------------------*)
(*4) Parameters to differentiate by (do NOT assign them values)*)
paramVars = {\[Delta], g, \[Rho], \[Gamma], p, jump};
baseline = {0.1, 0.2, 0.01, 0.3, 40,
0.0001}; (*{\[Delta],g,\[Rho],\[Gamma],p,jump}*)
eps = 10^-4;
(*-------------------------------------------------------------*)
(*5) Enforce u(t)>=0 (smooth projection for numerical stability)*)
useSmooth =
True; (*True recommended for robust ParametricNDSolveValue*)
kappa = 50; (*smoothness;larger->closer to Max[0,z]*)
uSmooth[z_] := (1/kappa) Log[1 + Exp[kappa z]]; (*softplus*)
uProj[z_] := Max[0, z];
uRule[lam_, vv_, pp_] :=
Module[{z = (pp - lam + vv)/\[Alpha]C},
```



19397445, 2026, 3, Downloaded from https://onlinelibrary.wiley.com/doi/10.1111/nrm.70037 by CochraneItalia, Wiley Online Library on [04/07/2026]. See the Terms and Conditions (https://onlinelibrary.wiley.com/terms-and-conditions) on Wiley Online Library for rules of use; OA articles are governed by the applicable Creative Commons License

```
If[useSmooth, uSmooth[z], uProj[z]]];

(*  ========================================
====*)

(*6) Define the 4 BVP systems*)

(*========================================
========*)

(*--OLNE ODEs (current-value)--*)

eqnsOLNE = {x'[t] ==

r[B[t]] x[t] (1 - x[t]/K) - n*uRule[\[Lambda][t], v[t], p],

B'[t] == g B[t] - \[Delta] Z[t] - jump,

Z'[t] ==

n*uRule[\[Lambda][t], v[t], p] - \[Gamma] Z[t], \[Lambda]'[

t] == \[Rho] \[Lambda][t] - \[Lambda][t] r[

B[t]] (1 - 2 x[t]/K), \[Mu]'[

t] == \[Rho] \[Mu][

t] - (\[Lambda][t] rprime[B[t]] x[t] (1 - x[t]/K) + g \[Mu][t]),

v'[t] == (\[Rho] + \[Gamma]) v[t] + \[Delta] \[Mu][t]};

(*--Regulator ODEs (planner;Choice 1:V2(x)=n Log x,V1(B)=n Sqrt B)--*)

eqnsRegulator = {x'[t] ==

r[B[t]] x[t] (1 - x[t]/K) - n*uRule[\[Lambda][t], v[t], p],

B'[t] == g B[t] - \[Delta] Z[t] - jump,

Z'[t] ==

n*uRule[\[Lambda][t], v[t], p] - \[Gamma] Z[t], \[Lambda]'[

t] == \[Rho] \[Lambda][

t] - (n/x[t] + \[Lambda][t] r[B[t]] (1 - 2 x[t]/K)), \[Mu]'[

t] == \[Rho] \[Mu][

t] - (n/(2 Sqrt[B[t]]) + \[Lambda][t] rprime[B[t]] x[

t] (1 - x[t]/K) + g \[Mu][t]),

v'[t] == (\[Rho] + \[Gamma]) v[t] + \[Delta] \[Mu][t]};

initBCs = {x[t0] == x0, B[t0] == B0, Z[t0] == Z0};

termStateBCs = {x[tf] == xF, B[tf] == BF, Z[tf] == ZF};

termCostateBCs = {\[Lambda][tf] == 0, \[Mu][tf] == 0, v[tf] == 0};

olneFixedEq = Join[eqnsOLNE, initBCs, termStateBCs];

olneFreeEq = Join[eqnsOLNE, initBCs, termCostateBCs];

regFixedEq = Join[eqnsRegulator, initBCs, termStateBCs];

regFreeEq = Join[eqnsRegulator, initBCs, termCostateBCs];

(*Sanity check:each has 6 ODEs+6 BCs=12 equations total*)

Print["Lengths (should all be 12): ",

Length /@ {olneFixedEq, olneFreeEq, regFixedEq, regFreeEq}];

(*========================================
========*)

(*7) Solve with ParametricNDSolveValue*)

(*========================================
========*)

(*Use shooting explicitly for BVP robustness*)

shootMethod = {"Shooting",

"ImplicitSolver" -> {"Newton", "StepControl" -> "LineSearch"}};

solOLNEFixed =

ParametricNDSolveValue[

olneFixedEq, {x, B, Z, \[Lambda], \[Mu], v}, {t, t0, tf},

paramVars, Method -> shootMethod, WorkingPrecision -> 30,

MaxSteps -> Infinity];

solOLNEFree =

ParametricNDSolveValue[

olneFreeEq, {x, B, Z, \[Lambda], \[Mu], v}, {t, t0, tf}, paramVars,

Method -> shootMethod, WorkingPrecision -> 30,

MaxSteps -> Infinity];

solRegFixed =

ParametricNDSolveValue[

regFixedEq, {x, B, Z, \[Lambda], \[Mu], v}, {t, t0, tf}, paramVars,

Method -> shootMethod, WorkingPrecision -> 30,

MaxSteps -> Infinity];

solRegFree =

ParametricNDSolveValue[

regFreeEq, {x, B, Z, \[Lambda], \[Mu], v}, {t, t0, tf}, paramVars,

Method -> shootMethod, WorkingPrecision -> 30,

MaxSteps -> Infinity];

(*========================================
=======*)
```



19397445, 2026, 3, Downloaded from https://onlinelibrary.wiley.com/doi/10.1111/nrm.70037 by CochraneItalia, Wiley Online Library on [04/07/2026]. See the Terms and Conditions (https://onlinelibrary.wiley.com/terms-and-conditions) on Wiley Online Library for rules of use; OA articles are governed by the applicable Creative Commons License

```
(*8) Build Sensitivity Functions (centered difference)*)

(*=========================================
======*)

makeSensCentered[sol_, varIdx_, parIdx_] :=

Function[{tt},

Module[{pPlus = baseline, pMinus = baseline},

pPlus[[parIdx]] += eps;

pMinus[[parIdx]] -= eps;

(((sol @@ pPlus)[[varIdx]][tt] - (sol @@ pMinus)[[varIdx]][

tt])/(2 eps))]];

scenarios = {"OLNE-Fixed", "OLNE-Free", "Regulator-Fixed",

"Regulator-Free"};

solList = {solOLNEFixed, solOLNEFree, solRegFixed, solRegFree};

(*Choose which states to plot/tabulate*)

statesLegend = {"x", "B",

"Z"}; (*Supporting Information S1: Figure 1 uses mainly x and B; keep Z if
desired*)

stateIdxs = Range[Length@statesLegend];

pparamsLegend = {"\[PartialD]/\[PartialD]\[Delta]",

"\[PartialD]/\[PartialD]g", "\[PartialD]/\[PartialD]\[Rho]",

"\[PartialD]/\[PartialD]\[Gamma]", "\[PartialD]/\[PartialD]p",

"\[PartialD]/\[PartialD](jump)" (*jump\[Congruent]\[CurlyPi] k*)};

sens = Table[

makeSensCentered[solList[[i]], j, k], {i, Length@solList}, {j,

Length@statesLegend}, {k, Length@paramVars}];

(*=========================================
========*)

(*9) Plot Grid of Sensitivities*)

(*=========================================
=======*)

plots = Table[

Plot[Evaluate@

Table[sens[[i, j, k]][t], {k, 1, Length@paramVars}], {t, t0, tf},

PlotLegends -> paramsLegend,

PlotLabel -> scenarios[[i]] <> " \[LongDash] " <> statesLegend[[j]],

ImageSize -> {420, 300}], {i, 1, Length@scenarios}, {j, 1,

Length@statesLegend}];

GraphicsGrid[plots, Spacings -> 2, ImageSize -> {1700, 1250}]

(*=========================================
========*)

(*10) Tables of Sensitivities at t=0,1,...,20*)

(*=========================================
======*)

tGrid = Range[t0, tf, 1];

Do[Print[

Style[scenarios[[i]] <> " \[LongDash] Sensitivities of " <>

statesLegend[[j]], Bold, 14]];

data =

Table[Prepend[Table[sens[[i, j, k]][tt], {k, 1, Length@paramVars}],

tt], {tt, tGrid}];

Print[Grid[Prepend[data, Join[{"Time"}, paramsLegend]],

Frame -> All, Spacings -> {1, 1}]];, {i, 1, Length@scenarios}, {j,

1, Length@statesLegend}];

(*=========================================
=======*)

(*11) Quantitative Sensitivity Summaries (optional,recommended)*)

(*-Peak absolute sensitivity over t in[0,T]*)

(*-Time-integrated absolute sensitivity (trapezoid rule)*)

(*=========================================
========*)

tFine = Range[t0, tf, 0.1];

dt = tFine[[2]] - tFine[[1]];

trapzAbs[f_] :=

Module[{vals = Abs[f /@ tFine]},

Total[(Most[vals] + Rest[vals])/2]*dt];

peakAbs[f_] := Max[Abs[f /@ tFine]];

peakTable =

Table[peakAbs[sens[[i, j, k]]], {i, Length@scenarios}, {j,

Length@statesLegend}, {k, Length@paramVars}];

intTable =
```



19397445, 2026, 3, Downloaded from https://onlinelibrary.wiley.com/doi/10.1111/nrm.70037 by CochraneItalia, Wiley Online Library on [04/07/2026]. See the Terms and Conditions (https://onlinelibrary.wiley.com/terms-and-conditions) on Wiley Online Library for rules of use; OA articles are governed by the applicable Creative Commons License

```
Table[trapzAbs[sens[[i, j, k]]], {i, Length@scenarios}, {j,
Length@statesLegend}, {k, Length@paramVars}];
Do[Print[
Style[scenarios[[i]] <> " \[LongDash] Peak |Sensitivity|", Bold,
14]];
Print[Grid[
Prepend[Table[
Prepend[peakTable[[i, j, All]], statesLegend[[j]]], {j,
Length@statesLegend}], Prepend[paramsLegend, "State"]],
Frame -> All]];
Print[Style[
scenarios[[i]] <>
" \[LongDash] \!\(\*SubsuperscriptBox[\(\[Integral]\), \(0\), \
\(T\)]\) |Sensitivity| dt", Bold, 14]];
Print[Grid[
Prepend[Table[
Prepend[intTable[[i, j, All]], statesLegend[[j]]], {j,
Length@statesLegend}], Prepend[paramsLegend, "State"]],
Frame -> All]];, {i, 1, Length@scenarios}];
(*=========================================
======================*)
(*Notes:-If you want exact projection u=Max[0,z],set useSmooth=False.\
For numerical stability in BVP+perturbations,keep useSmooth=True.
-Supporting Information S1: Figure 1 focuses on x(t) and B(t);you can
set statesLegend={"x",
"B"} to generate exactly the 2-column figure grid.*)
(*=========================================
======================*).
```



19397445, 2026, 3, Downloaded from https://onlinelibrary.wiley.com/doi/10.1111/nrm.70037 by CochraneItalia, Wiley Online Library on [04/07/2026]. See the Terms and Conditions (https://onlinelibrary.wiley.com/terms-and-conditions) on Wiley Online Library for rules of use; OA articles are governed by the applicable Creative Commons License